NASA CONTRACTOR REPORT

NASA CR-1698

TECHNIQUES FOR EVALUATING THE SOUND ABSORPTION OF MATERIALS AT HIGH INTENSITIES

by John G. Powell and John J. Van Houten

Prepared by
LTV RESEARCH CENTER, WESTERN DIVISION
LING-TEMCO-VOUGHT, INC.
Anaheim, Calif. 92803
for Langley Research Center

NATIONAL AERONAUTICS AND SPACE ADMINISTRATION • WASHINGTON, D. C. • JANUARY 1971

1. Report No.	2. Government Accession No.	3. Recipient's Catalog No.
NASA CR-1698		

4. Title and Subtitle	5. Report Date
TECHNIQUES FOR EVALUATING THE SOUND ABSORPTION OF MATERIALS AT HIGH INTENSITIES	January 1971
	6. Performing Organization Code
7. Author(s)	8. Performing Organization Report No.
John G. Powell and John J. Van Houten	N/A
	10. Work Unit No.
9. Performing Organization Name and Address	
LTV Research Center Western Division 1859 South Manchester Avenue Anaheim, California 92803	11. Contract or Grant No. NAS1-8763
	13. Type of Report and Period Covered Contractor Report
12. Sponsoring Agency Name and Address	
National Aeronautics and Space Administration Washington, D.C. 20546	14. Sponsoring Agency Code

15. Supplementary Notes

16. Abstract

Two unique methods applicable to evaluation of the sound absorption characteristics of materials have been investigated. The effort concentrated on methods suitable for evaluating materials under consideration for sound reduction treatment in jet engine nacelles. Since many sound absorbing materials become non-linear at the sound intensities encountered in the intake and fan exhaust ducts, a need exists for a convenient method of testing at these intensities in the laboratory. Both techniques evaluated during this study are capable of fulfilling this requirement. The methods investigated involve a tone-burst technique and a shock-tube procedure.

17. Key Words (Suggested by Author(s))	18. Distribution Statement
Sound absorption Shock tube Tone-burst	Unclassified - Unlimited

19. Security Classif. (of this report)	20. Security Classif. (of this page)	21. No. of Pages	22. Price*
Unclassified	Unclassified	77	$3.00

*For sale by the National Technical Information Service, Springfield, Virginia 22151

TABLE OF CONTENTS

TECHNIQUES FOR EVALUATING THE SOUND ABSORPTION OF MATERIALS AT HIGH INTENSITIES

By John G. Powell and John J. Van Houten

LTV Research Center, Western Division
Ling-Temco-Vought, Inc.

SUMMARY

Two unique methods applicable to evaluation of the sound absorption characteristics of materials have been investigated. The effort concentrated on methods suitable for evaluating materials under consideration for sound reduction treatment in jet engine nacelles. Since many sound absorbing materials become non-linear at the sound intensities encountered in the intake and fan exhaust ducts, a need exists for a convenient method of testing at these intensities in the laboratory. Both techniques evaluated during this study are capable of fulfilling this requirement. The methods investigated involve a tone-burst technique and a shock-tube procedure.

A tone-burst technique has been successfully employed to evaluate various types of materials from 500 Hz to 10,000 Hz. This technique provides sound pressure levels significantly higher than may be achieved by use of the impedance tube method of absorption measurement.

In this technique, a narrow bandwidth tone burst is propagated down a tube which is terminated first with a rigid surface, then with a sample of the absorptive material. A wall-mounted

microphone is used to measure the pulse amplitude before and after teflection from the tube termination. This data is then used to determine the normal incidence absorption coefficient.

Spectral data is obtained with this method by filtering a sinusoidal tone burst. The passband of the one-third octave filter coincides closely with the central lobe of the frequency spectrum of a tone burst of eight-cycle duration. Therefore, the filtered tone burst is a narrow-band pulse, the pulse width in this case being one-third octave.

Several methods of using the shock tube to perform high-intensity absorption measurements were investigated. The most promising involves the generation of a shock wave produced by rupturing a diaphragm in a shock tube and the expansion of the wave through an exponential area transformation. This weakens the shock strength, thereby circumventing problems associated with the large pressure jump encountered in the normal shock tube. The absorption coefficient of a sample of material placed in the end of the tube is determined by comparing the ratio of the reflected to incident pressure jump with the ratio measured for a rigid end termination.

INTRODUCTION

Sound pressure levels in the inlet duct of commercial fan jet aircraft can easily exceed 170 dB (ref. 1). It has been shown both theoretically (ref. 2) and experimentally (refs. 3 and 4) that the sound absorption characteristics of materials under consideration for treating these fan ducts become non-linear at sound levels significantly below this level. Therefore, a need exists for a convenient laboratory method of evaluating these materials at high sound levels, and it is toward this end that this program has been directed.

One of the most common duct lining concepts currently under consideration for use in jet engines consists of a thin sheet of absorbing material supported by a honeycomb structure, which is backed by an impervious sheet of aluminum. The absorbing material is most commonly a felted or woven metal cloth, or fiberglass reinforced epoxy or polyimid, or other similar material. This structure forms a resonant absorber on the order of one inch thick. The absorber typically becomes non-linear at sound pressure levels of from 120 dB to 160 dB, depending primarily upon the absorbing material and frequency.

The most commonly used method of evaluating these absorbers in the laboratory is the impedance tube in conjunction with flow resistance measurements. A flow duct interconnecting two reverberation chambers has been used (ref. 5) to perform full-scale measurements in the presence of flow. These methods, however, are not generally capable of reproducing the high sound pressure levels encountered in the fan ducting, and hence do not reveal the non-linear characteristics of the absorber.

Two methods which are capable of measuring the sound absorption of duct lining samples at the high sound intensities desired were studied during this program. One of these is a tone-burst technique, and the other utilizes a shock tube. In the tone-burst technique, a narrow bandwidth tone burst is reflected from the sample, and the absorption coefficient is determined from the reduction in amplitude of this pulse. The use of a tone burst has several advantages, the one most pertinent to this application being that the rated power handling capability of the electroacoustic sound source can be exceeded by a factor of ten. For example, loudspeakers rated at 40 watts have been driven with tone bursts of 600 watts peak without damage to the units. The maximum sound pressure capability is thus increased significantly. Commercially available equipment was used throughout this program; considerably higher levels could be expected for modified or specially designed equipment.

The other method, which utilizes a shock tube, produced pressures that were too high, resulting in data so far in the non-linear region that the results could not be reconciled with impedance tube or tone-burst data. However, a technique for expanding the shock front, thereby weakening it, was considered briefly. This approach shows considerable promise, but further investigations along this line would have been beyond the scope of the current study.

These methods are described in this report, which is broken down into several main sections. First, the impedance tube used as a standard for comparison is briefly described.

The next two sections describe the tone-burst tube and shock tube techniques. Both sections begin with a general description of the technique, followed by a theoretical discussion. The section on the tone-burst tube then describes some experimental details, and both sections conclude with examples of absorption data gathered by the respective techniques. Conclusions are presented in the final section.

TONE-BURST TUBE MEASUREMENTS

General Description of the Technique

In this experiment, an electrodynamic driver is attached to one end of a tube and a sample holder to the other. A microphone is mounted through the tube wall at any one of several stations located between the driver and the mid-section of the tube. The acoustic signal is a sound pulse consisting of a filtered tone burst.

To make an absorption measurement, the sample end of the tube is first terminated in a rigid metal surface. The ratio of the reflected to incident pulse amplitude for this case is used to calibrate the tube. The rigid termination is then replaced by a sample and the measurement is repeated. The calibration data is used to eliminate the effects of tube losses and the absorption coefficient of the sample is established from the two sets of measurements.

Single pulses have a broad frequency spectrum. However, it is possible to produce a narrow band pulse which readily lends itself to the gathering of absorption data. Such a pulse is generated by passing the output of a tone-burst generator through a band pass filter centered at the tone burst frequency. The tone-burst generator output in this case is essentially a single sinusoidal burst, beginning at the signal zero crossing, continuing at constant amplitude and frequency for a pre-selected number of cycles, and stopping at zero crossing. As will be discussed in detail later, with a proper selection of

parameters, only the center lobe of the tone-burst frequency spectrum is passed by the filter, resulting in a narrow band pulse.

Theoretical Considerations

To obtain the absorption coefficient from the tone-burst tube measurement, it is necessary to eliminate the effect of tube losses from the measured data. This can be accomplished by performing a measurement with a rigid end termination, and then repeating the measurement with a sample of absorptive material in the end.

It will be assumed that α, the normal incidence energy absorption coefficient, is zero for the tone burst tube with a rigid metal end termination. This has been shown to be a valid assumption within experimental error from measurements made with a microphone located five to ten wavelengths from the end of the tube. Therefore, we can use empty tube measurements to determine tube propagation loss directly.

Referring to Figure 2, we make the following definitions:

$W(x,t)$ = energy in the tone burst with the tube empty (rigid end ② termination)

$E(x,t)$ = energy in the tone burst for the tube with a material sample at location ②

Subscript i refers to a pulse traveling from position ① to position ② (incident)

Subscript r refers to a pulse traveling in the direction from ② to ① (reflected)

Subscripts 1 and 2 refer to quantities as they would be measured at positions ① and ②, respectively.

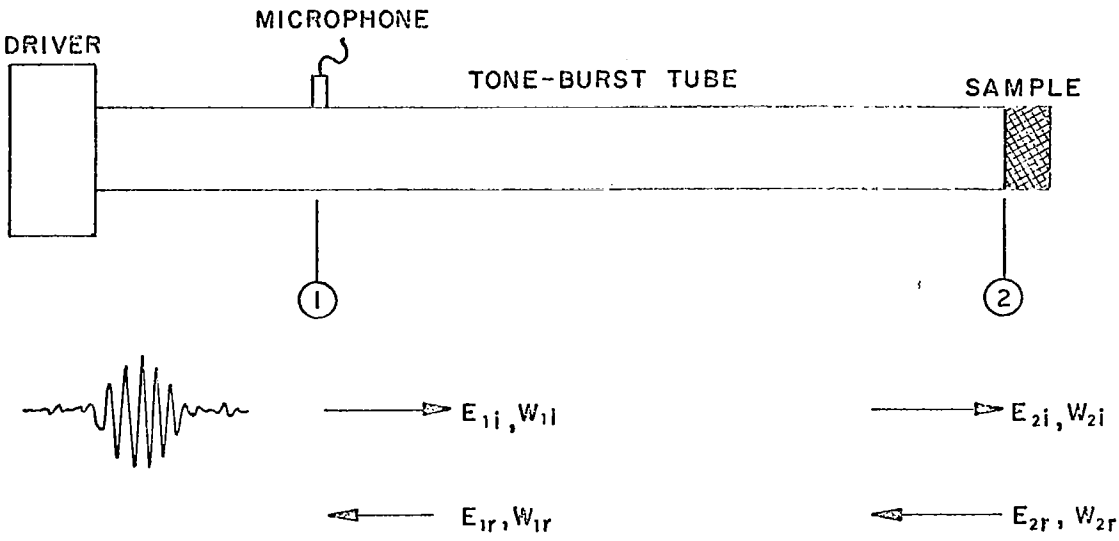

FIGURE 2 EVENTS IN THE TONE BURST TUBE

The energy lost by the pulse while propagating down the tube from 2 to 1 (or from 1 to 2) is independent of the tube termination. Expressing this mathematically,

$$\frac{E_{1r}}{E_{2r}} = \frac{W_{1r}}{W_{2r}} \tag{1}$$

Dividing the numerator of both sides of this equation by E_{1i} and the denominator by E_{2i},

$$\frac{\frac{E_{1r}}{E_{1i}}}{\frac{E_{2r}}{E_{2i}}} = \frac{\frac{W_{1r}}{E_{1i}}}{\frac{W_{2r}}{E_{2i}}} \tag{2}$$

The quantities in this relation have the following physical meaning:

$\frac{E_{1r}}{E_{1i}} = R_s$ the ratio measured at the microphone with a sample in the end of the tube

$\frac{E_{2r}}{E_{2i}} = R$ the desired energy reflection coefficient of the sample ($R = 1-\alpha$)

In the actual experiment we are free to set the incident level at the microphone equal for both the rigid and sample tube terminations; hence,

$$E_{1i} = W_{1i}. \tag{3}$$

With the levels adjusted so that (3) holds, we also have

$$E_{2i} = W_{2i} \tag{4}$$

Using (3),

$$\frac{W_{1r}}{E_{1i}} = \frac{W_{1r}}{W_{1i}} = R_o,$$

the ratio measured at the microphone with the rigid tube termination. And finally, using (4),

$$\frac{W_{2r}}{E_{2i}} = \frac{W_{2r}}{W_{2i}} = 1,$$

since this is the energy reflection coefficient of the rigid termination and was assumed to be unity. Rewriting equation (2) in terms of the measured ratios R_o and R_s and the desired reflection coefficient R,

$$\frac{R_s}{R} = \frac{R_o}{1}$$

or, since energy is proportional to pressure squared,

$$R = \frac{R_s}{R_o} = \left(\frac{P_{rs}}{P_{is}} \times \frac{P_{io}}{P_{ro}}\right)^2 = \left(\frac{P_{rs}}{P_{ro}}\right)^2$$

where the subscripts i and r refer to incident and reflected pressure pulses and s and o refer to a sample or rigid termination, respectively. The last step follows since $P_{is} = P_{io}$. Thus, the sample reflection coefficient is simply the square of the ratio of the reflected pulse amplitudes with and without a sample in the tube. The normal incidence energy absorption coefficient of the sample is therefore given by

$$\alpha_s = 1 - \left(\frac{P_{rs}}{P_{ro}}\right)^2 \qquad (5)$$

The technique must be capable of providing the absorption coefficient as a function of frequency. A transient signal contains a broad band frequency spectrum so that narrow band frequency data can be obtained by filtering the reflected signal, looking at a narrow bandwidth. However, if the drive signal applied to an electrodynamic transducer contained broad band components, the sound pressure obtainable in any narrow frequency band would be severely limited. Hence, it is desirable to use a narrow bandwidth pulse for the drive signal. Such a signal is described in the following paragraph.

Tone burst signals of four and eight-cycle duration are shown in Figure 3, where T is the period of the sine wave and N the number of cycles in the tone burst. Those signals are described analytically by the function

$$f(t) = \begin{cases} \sin \omega_o t, & 0<t<NT \\ 0 \text{ elsewhere} \end{cases} \qquad (6)$$

where ω_o is the angular frequency of the sinusoidal wave form.

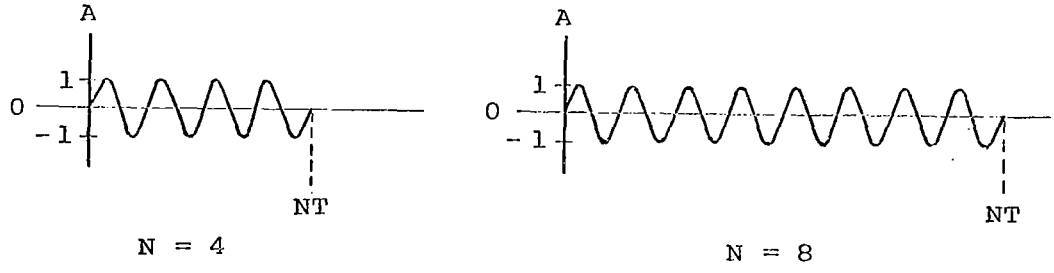

FIGURE 3. TONE BURST SIGNALS

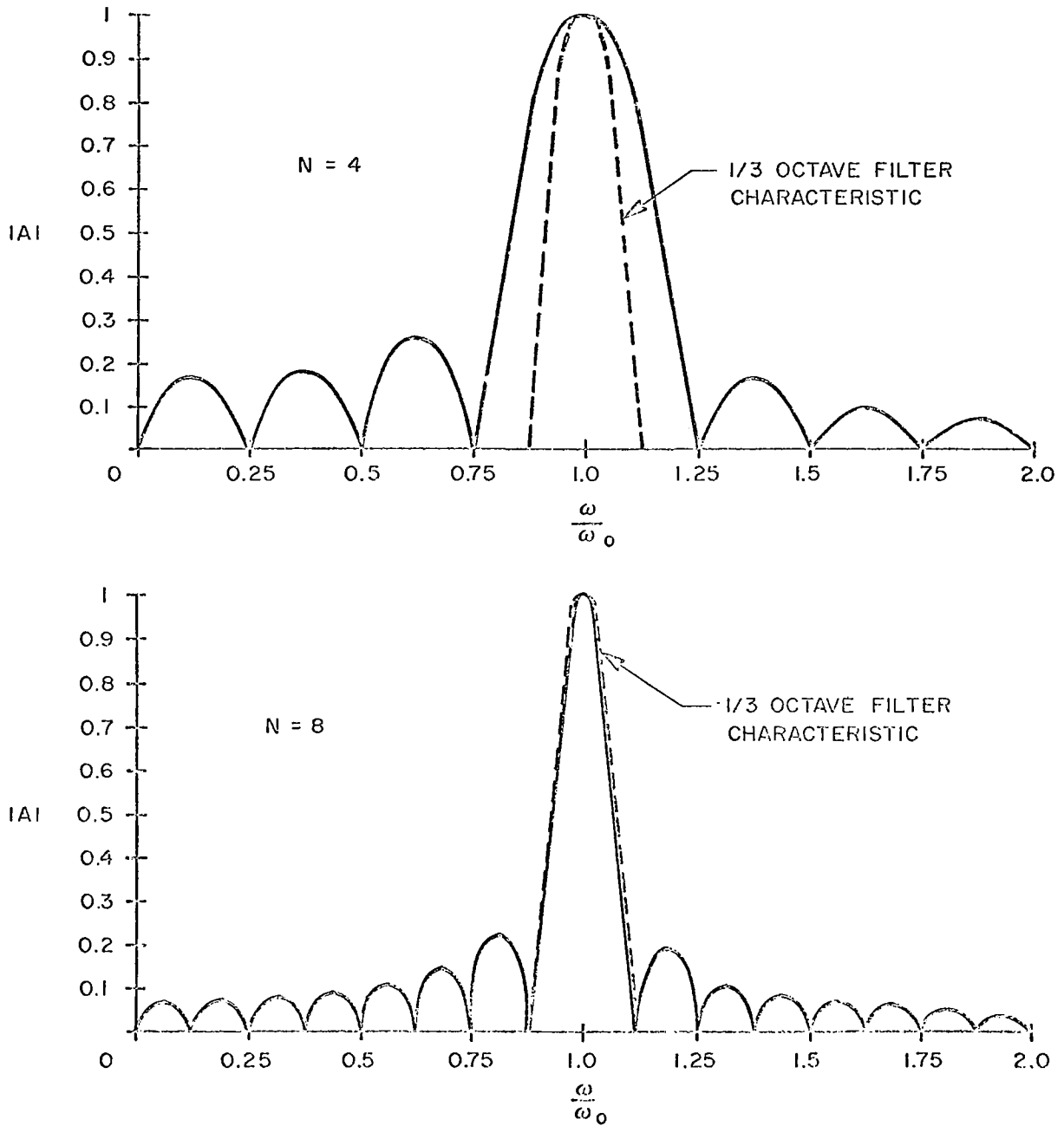

FIG. 4 FREQUENCY SPECTRUM OF SINUSOIDAL TONE BURSTS OF 4 AND 8 CYCLE DURATION

59-101

The frequency spectrum can be found by taking the Fourier cosine transform:

$$F(\omega) = \int_0^{NT} f(t)\cos\,\omega t\,dt = \int_0^{Nt} \cos\omega_o t\cos\omega t\,dt$$

$$= \frac{N\pi}{\omega_o}\left[\frac{\sin x}{x} - \frac{\sin y}{y}\right] \qquad (7)$$

where

$$x = \frac{N\pi}{\omega_o}\left(\omega_o - \omega\right) \text{ and } y = \frac{N\pi}{\omega_o}\left(\omega_o + \omega\right)$$

This function is plotted in Figure 4 for N = 4 and N = 8. A B&K one-third octave filter characteristic is superimposed on these spectra in dashed lines. It illustrates that the one-third octave filter contains essentially only the main lobe of the tone burst frequency spectrum, for N = 8. For this case the tone burst is a narrow band pulse, the pulse width being one-third octave. To further define the signal we shall consider the effect of one-third octave filtering on this tone burst. For experimental application, this is an ideal bandwidth since it corresponds to commercially available filtering characteristics.

Let the signal f(t) be passed through the ideal band pass filter with transfer function H (ω) shown below.

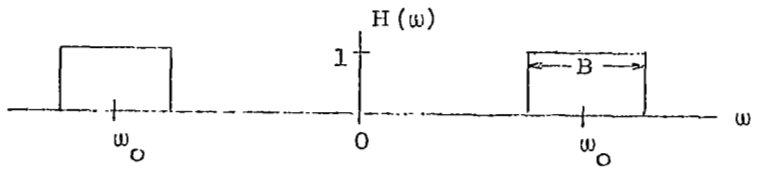

FIGURE 5. IDEAL BAND PASS FILTER

The output function g(t) is given by the inverse Fourier transform

$$g(t) = \frac{1}{2\pi}\int_{-\infty}^{\infty} F(\omega)H(\omega)\exp(i\omega t)\,d\omega$$

To avoid the difficulties which would be encountered in evaluating this integral, a narrow band approximation to $F(\omega)$ is used. Let

$$F(\omega)\approx\widetilde{F}(\omega) = \begin{cases} \dfrac{\sin\,(\omega-\omega_b)T}{\omega-\omega_b}, & \left(\omega_b - \dfrac{B}{2}\right) \le \omega \le \left(\dfrac{B}{2} + \omega_b\right) \\ \dfrac{\sin\,(\omega+\omega_b)T}{\omega+\omega_b}, & \left(-\omega_b - \dfrac{B}{2}\right) \le \omega \le \left(\dfrac{B}{2} - \omega_b\right) \\ 0 \quad \text{elsewhere} \end{cases}$$

and note that $\widetilde{F}(\omega)$ is given by (reference 6)

$$\widetilde{F}(\omega) = \left\{ \begin{array}{l} 2\sin\omega t, -\dfrac{B}{2} \le \omega \le \dfrac{B}{2} \\ 0 \text{ elsewhere} \end{array} \right\} \circledast \pi\delta\left[(\omega-\omega_o) + (\omega+\omega_o)\right]$$

where $\circledast$ denotes convolution and δ is the delta function. The output function g(t) is now found from the inverse Fourier transform of $\widetilde{F}(\omega)$:

$$g(t) = \frac{1}{\pi}\left[\int_0^{\frac{B}{2}} \frac{2\sin\omega T}{\omega}\cos\omega t\,d\omega\right]\cos\omega_b t.$$

Evaluation of this integral yields

$$g(t) = \frac{1}{\pi}\left\{ Si\left[\frac{B}{2}(t+T)\right] - Si\left[\frac{B}{2}(t-T)\right]\right\}\cos\omega_o t \qquad (8)$$

where Si(x) is the sine integral function

$$Si(x) = \int_0^x \frac{\sin x}{x}\, dx$$

A computer program was written to calculate g(t) based on the series expansion of Si(x). The results of this computation for N = 4 and N = 8, with the center frequency equal to 2 kHz and the one-third octave filter bandwidth assumed for this purpose to be 466 Hz is shown in Figure 6. This can be compared with Figure 13-b which is an oscilloscope photograph for N = 8.

Definition of Peak Pressure Level

Before proceeding, it is necessary to define peak pressure level (PPL). Normally, the term sound pressure level (SPL), is used to describe pressure levels. However, this is based on an rms value which has no meaning when describing pressures of the type being considered here. These pressures are discontinuous functions of time. Furthermore, in the case of the shock tube discussed in a later section, they are not symmetrical with respect to the ambient pressure and are not periodic in time. The periodicity evident in oscilloscope photographs of a shock tube is determined solely by tube length and sensor location, and is not related in any way to the frequency content of the input pressure function.

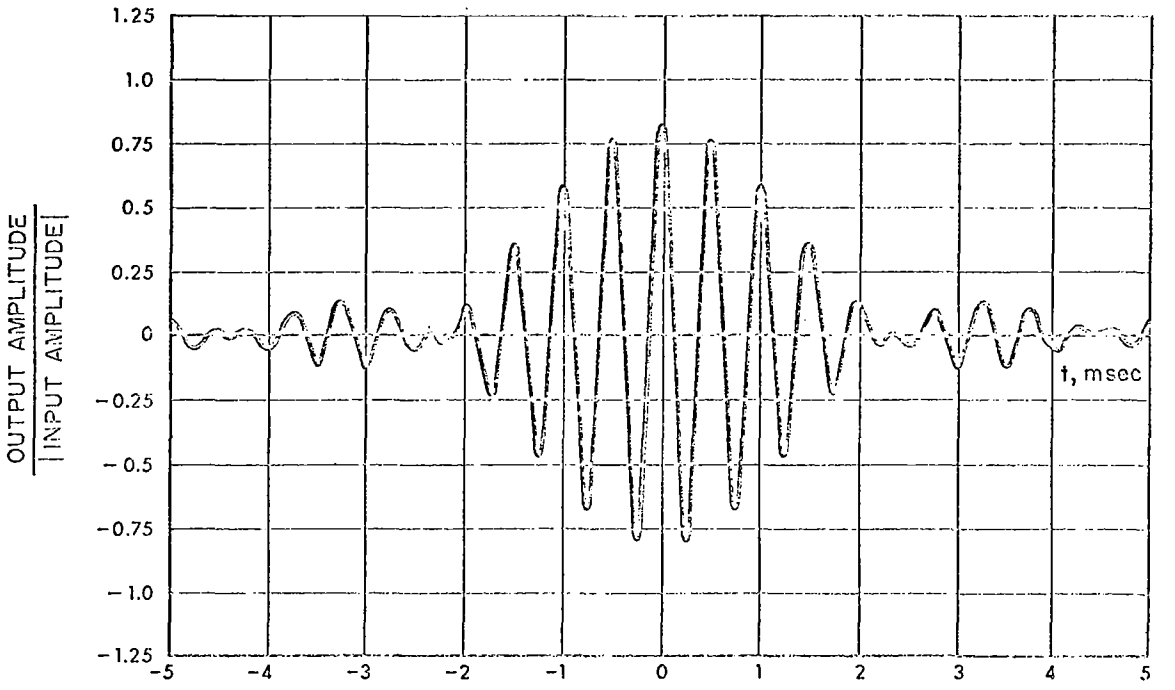

A. 4 CYCLE TONE BURST INPUT

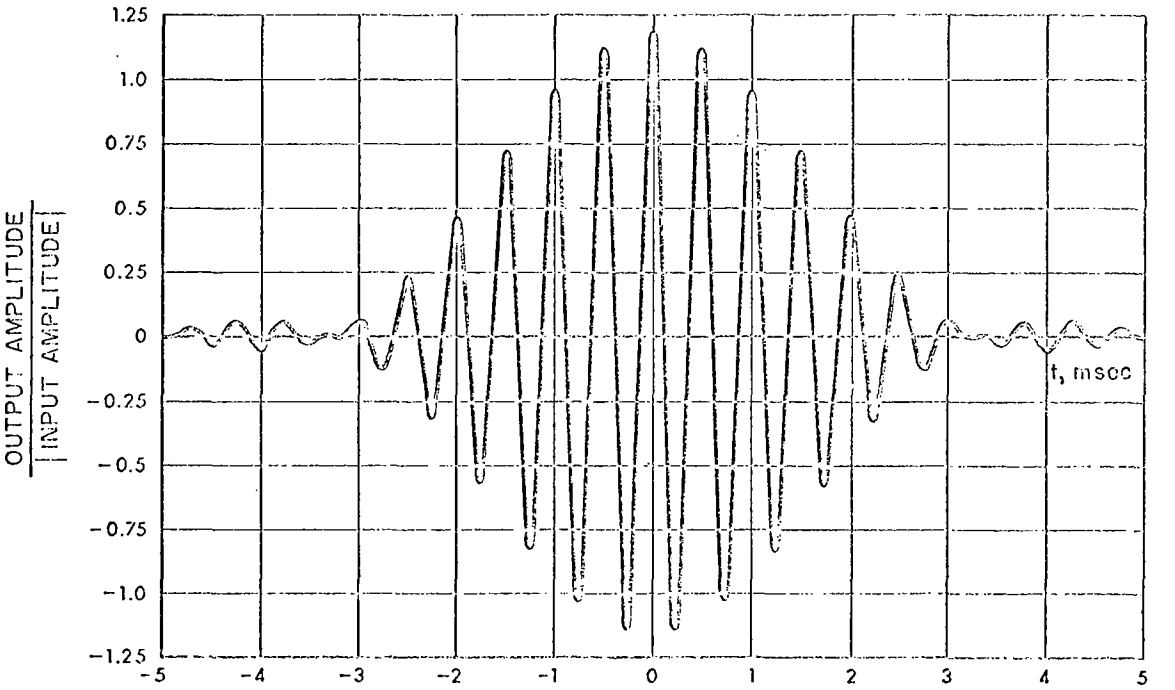

B. 8 CYCLE TONE BURST INPUT

FIG. 6. ONE-THIRD OCTAVE FILTER OUTPUT FOR TONE BURST, ASSUMING AN IDEAL BANDPASS FILTER. THE SIGNAL OCCURRING BEFORE APPROXIMATELY -2.3 MSEC IN A. AND -3.3 MSEC IN B. IS A RESULT OF THE APPROXIMATION. (SEE TEXT)

Determination of an "rms" value for a signal involves evaluation of an integral of the form

$$\sqrt{\frac{1}{T}\int_0^T p(t)^2 dt}$$

where p(t) is the pressure function and T is the period of a repetitive signal or the duration of a pulse. Obviously, the peak pressure is not related to the "rms" pressure for a non-recurrent pulse, the latter depending only on the magnitude of the area under the pressure-time curve, not on the amplitude.

We will, therefore, use the term peak pressure level, abbreviated PPL, to describe the pressure amplitude and define this as 20 log of the zero-to-peak pressure of the primary shock wave or of the zero-to-peak pressure of the maximum value of the filtered tone burst envelope, relative to 0.0002 dynes/cm^2.

Experimental Procedure

The signal described in Equation (8) is realized in practice as follows. Referring to Figures 7 and 8, the output from a sine wave oscillator supplies the signal to a commercially available tone-burst generator. The tone-burst generator is essentially an electronic gate that switches on the sine wave at a positive going zero crossing and switches it off again at a positive going zero crossing after a selected number of cycles. When this tone burst is fed through a one-third octave band pass filter, the resulting signal appears as shown in Figures 7 and 14. The counter is used to set the oscillator frequency precisely to the filter center frequency. The filter cannot respond instantaneously, so the envelope of the output signal from the filter has a gradual rise and fall. The total pulse duration is a function of both the number of cycles in the tone burst and the filter characteristics. This signal is amplified and applied to the electrodynamic loudspeaker which generates the desired acoustic pulse. This pulse propagates down the tube past the microphone to the sample where it is reflected. The reflected pulse then travels up and down the tube, reflecting off the driver and sample until the energy is dissipated. The microphone output is passed through another identical filter and read out on an oscilloscope.

In order to read the amplitudes of the incident and first reflected pulse accurately, a differential comparator is used in conjunction with the oscilloscope. With this unit, an offset voltage is applied so that a 11-volt signal, for instance, can be read at a deflection factor of 1Mv/cm. With this approach the resolution in signal amplitude is limited only by system noise.

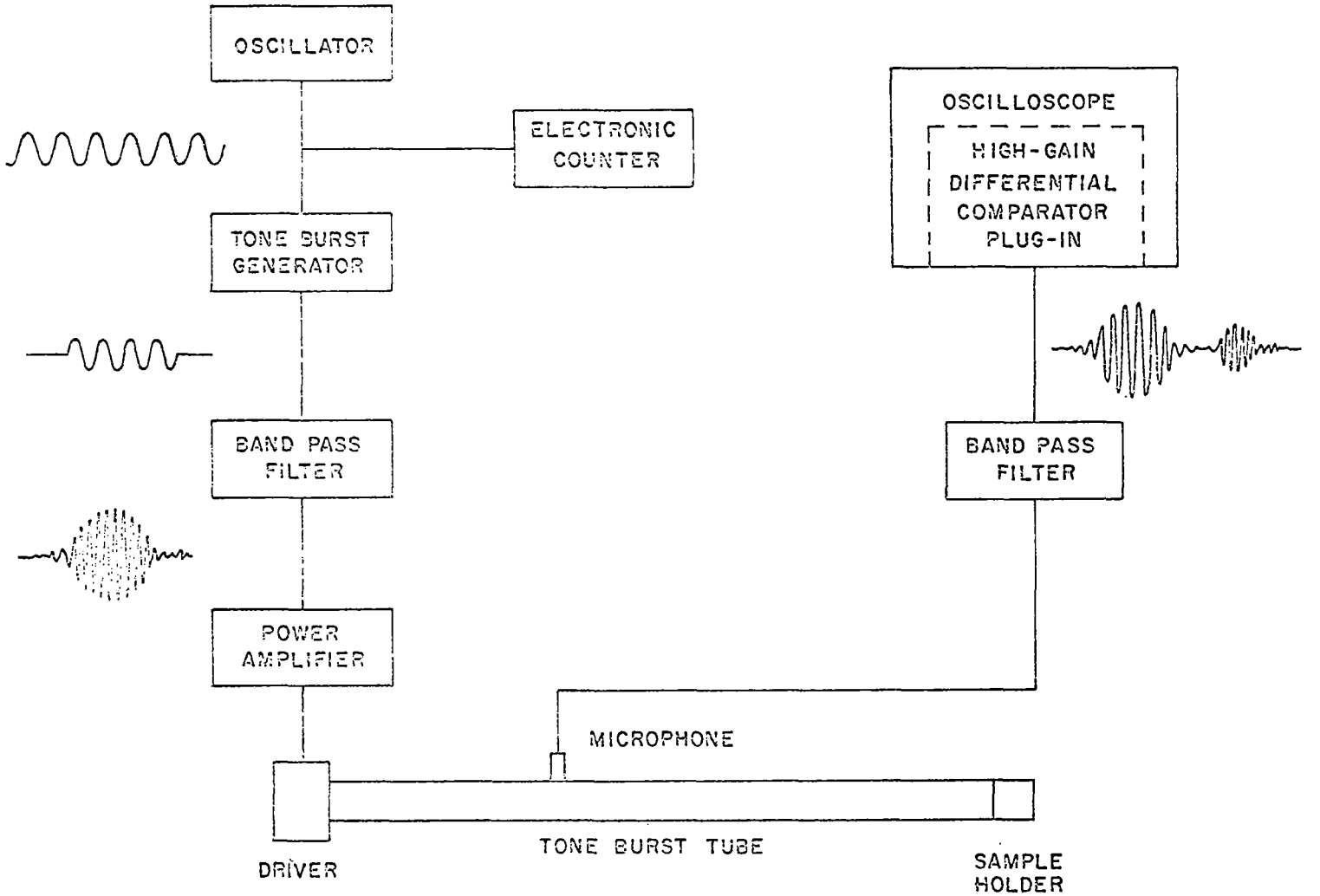

FIG. 7. BLOCK DIAGRAM — TONE BURST TUBE ABSORPTION MEASUREMENT

FIGURE 7.

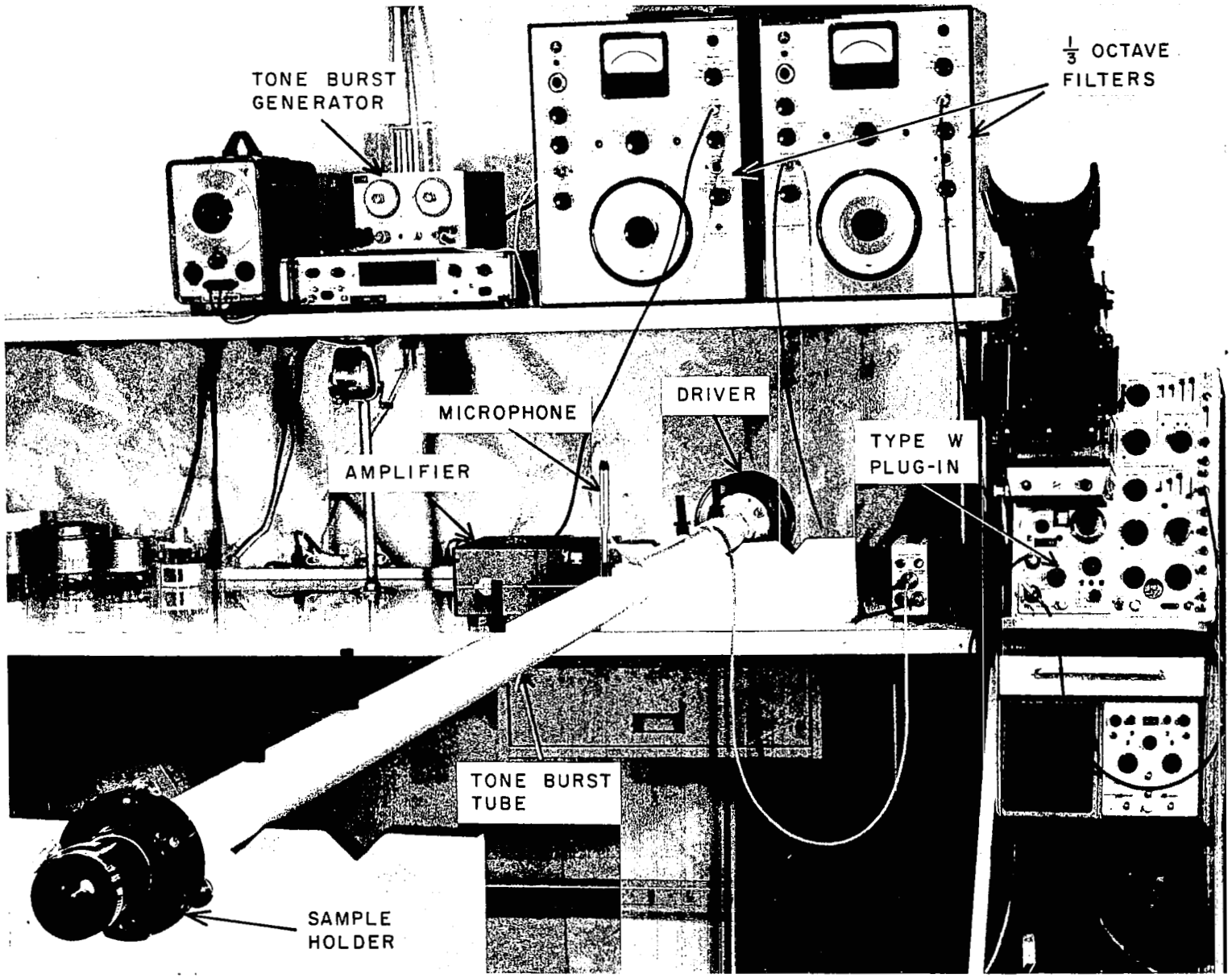

FIG. 8. TONE BURST TUBE

In this experiment most measurements were made with the number of cycles, N, in the tone burst equal to 8, since the pass band of the one-third octave filters coincides almost exactly with the central lobe of the frequency spectrum of this signal. However, at low frequencies (400 Hz and 500 Hz), with a 20-foot long tube, the incident and reflected pulses overlap for N = 8, so that these data were taken with N = 4. The disadvantage of using N = 4 is that the filter frequency characteristic cuts through the steep slope of the main lobe of the tone-burst spectrum, making the signal level sensitive to small shifts in oscillator frequency.

For a given value of N, there is a minimum tube length which will space the incident pulse and the pulse reflected from the sample far enough apart so that they do not overlap sufficiently to alter the apparent pulse amplitudes. The arrival time of the reflection off the driver is also of concern but since it is of lower amplitude, a greater degree of overlap can be tolerated before the accuracy is degraded. In general, the driver-to-microphone spacing should be about one-third of the tube length. This situation worsens as the frequency is decreased since the subsequent pulses are of more nearly the same amplitude and since, for constant N, the pulse duration increases. An empirically determined minimum tube length as a function of frequency is shown in Figure 9 for N = 4 and N = 8. For the data gathered in this program, tube lengths of 20 feet, 10 feet, and 5 feet were used to span the frequency range from 400 Hz to 10 kHz.

Tube diameter influences the measurements in two important ways: attenuation of the pulse within the tube increases as the diameter decreases, and the tube diameter must remain smaller than about a half wavelength to maintain a plane wave. Obviously, it is desirable to minimize tube length so as to maximize the pulse

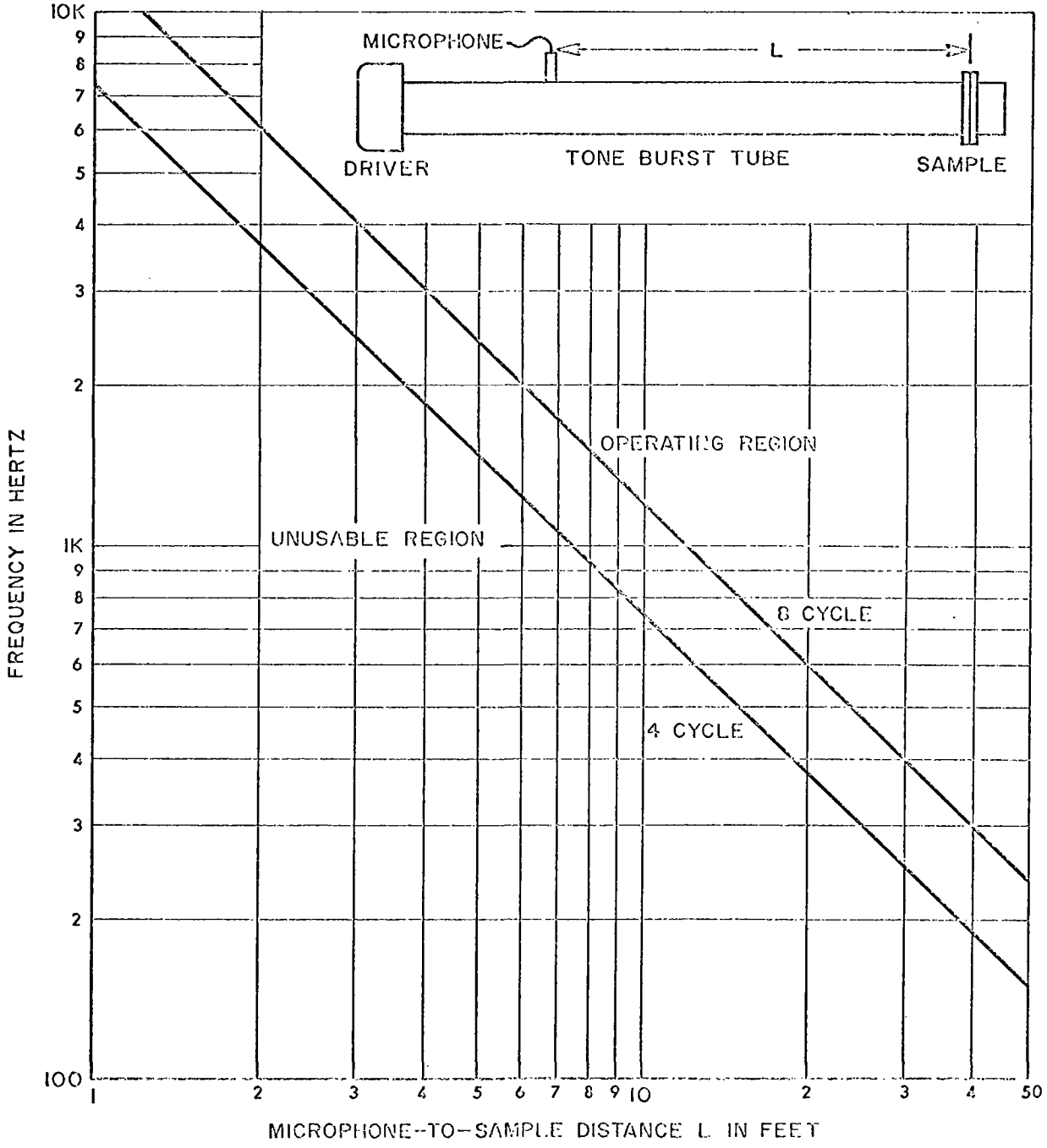

FIG. 9 MINIMUM TUBE LENGTH VS FREQUENCY FOR THE ONE-THIRD OCTAVE FILTERS USED IN THIS EXPERIMENT. 4 AND 8 CYCLE TONE BURSTS.

amplitude capability at the sample surface. Figures 10 and 11 show measured values of sound attenuation in the tubes used in this experiment; Figure 10 for a 2-inch diameter tube and Figure 11 for a 3/4-inch diameter tube. Note that in both cases the attenuation rate becomes nonlinear for peak pressure levels (PPL) above 140 dB.

These attenuation rates were determined from measured incident and reflected tone-burst levels in the empty tube by assuming: 1) the reflection coefficient of the rigid end termination is unity, and 2) the attenuation follows the relation

$$p = p_o e^{-\beta x}$$

where p is the PPL of the tone burst. These data clearly show that significantly higher incident PPL's can be obtained by maximizing tube diameter and minimizing tube length, particularly at high frequencies and PPL's. As an example, at 160 dB PPL and 4 kHz, an increase of 5 dB could be realized by reducing the tube length from 10 feet to 5 feet, and almost an additional 4 dB could be realized by increasing tube diameter from 3/4-inch to 2 inches, for a net increase of nearly 9 dB at the sample surface.

The maximum PPL at the sample surface achieved with optimized tube dimensions, for the particular amplifier and driver used in this experiment is shown in Figure 12. It is seen that this maximum level varies from 166 dB at 500 Hz to 158 dB at 10 kHz.

When the output from the tone-burst generator is applied to the filter, the envelope of the resulting pulse is determined solely by the filter characteristics for a given value of N. The pulse amplitude builds up slowly to its maximum value, and continues

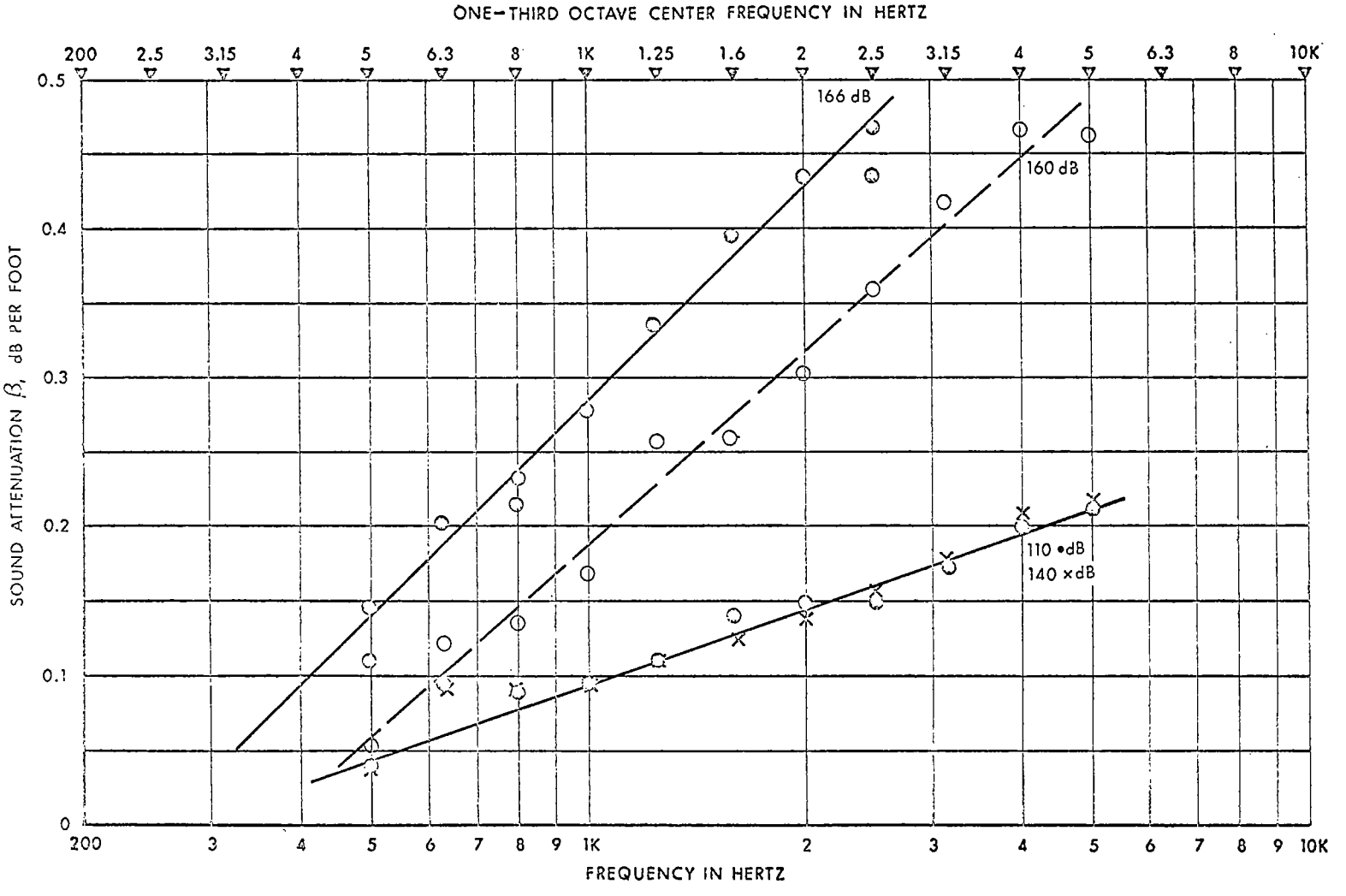

FIG. 10 SOUND ATTENUATION IN A 2 INCH DIAMETER TUBE AS A FUNCTION OF SOUND INTENSITY

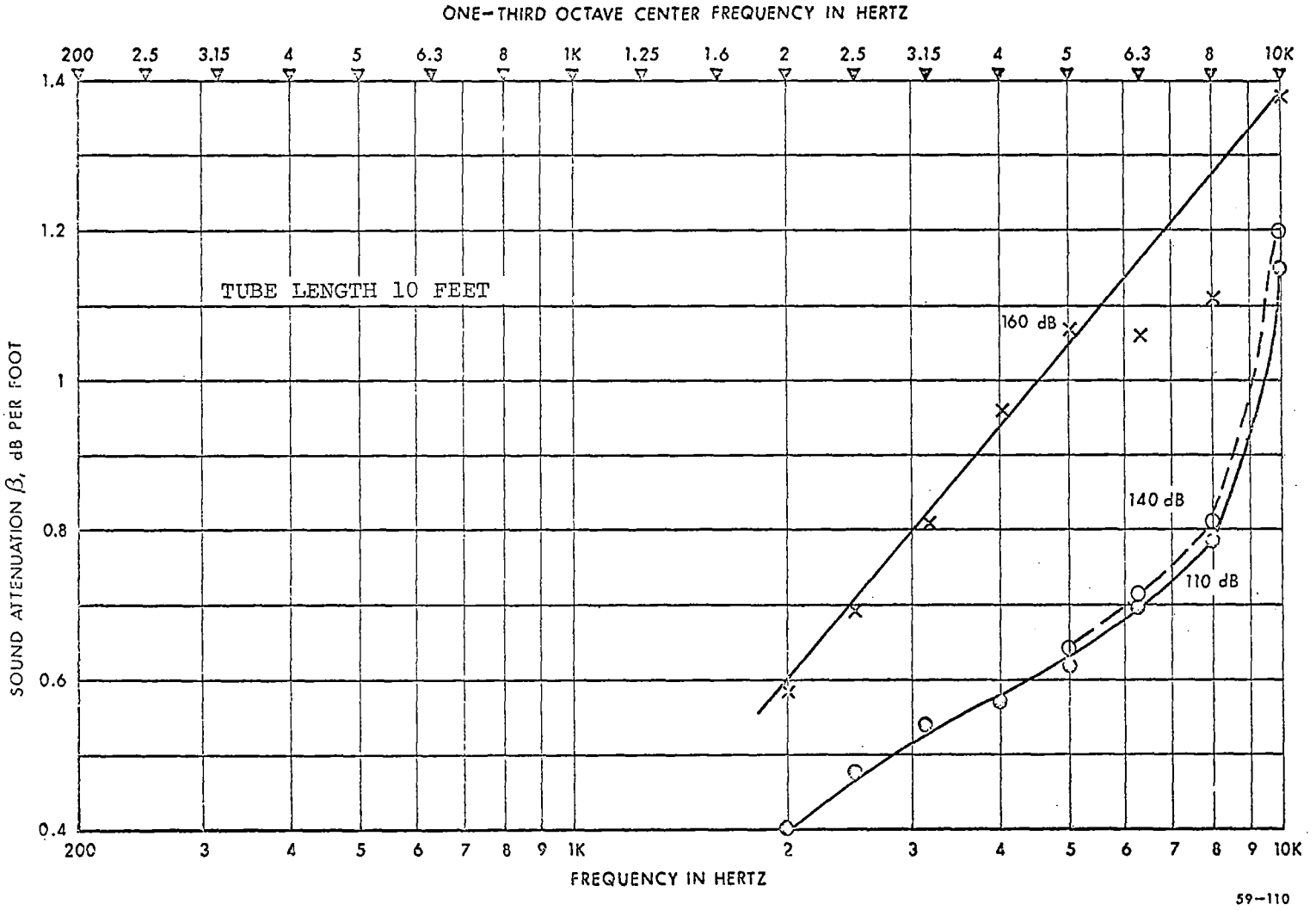

FIG. 11 SOUND ATTENUATION IN A 3/4 INCH DIAMETER TUBE AS A FUNCTION OF SOUND INTENSITY

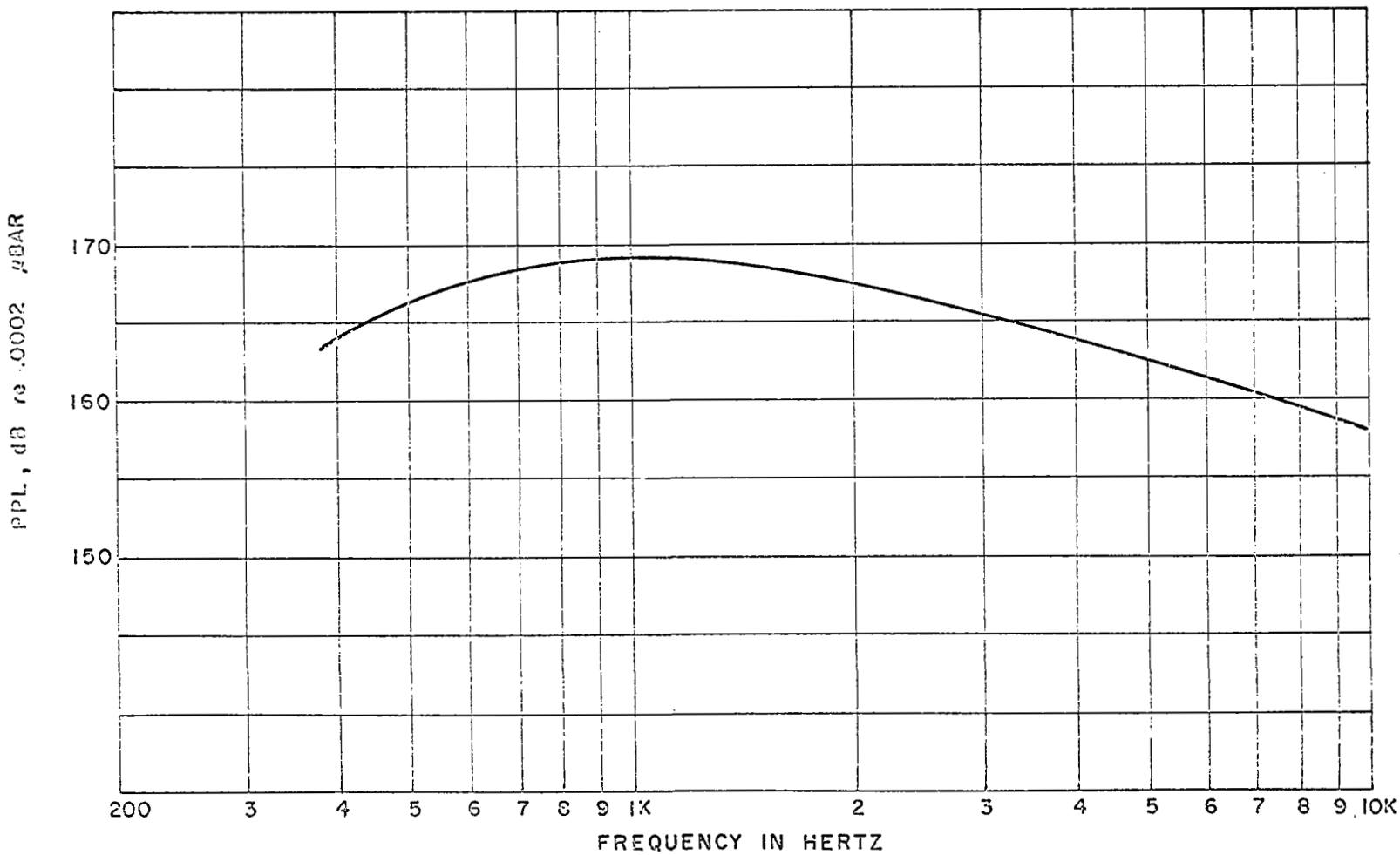

FIG. 12. MAXIMUM PPL INCIDENT ON ABSORPTIVE SAMPLE FOR OPTIMIZED TUBE DIMENSIONS

with decreasing amplitude after the tone burst is switched off. The filter used (B&K Type 2112 Audio Frequency Spectrometer) is of a very high order (maximum slope about one hundred dB/ octave) so that an exact analytical description of the resulting signal is very difficult. However, a close approximation can be obtained by assuming the filter is ideal, with an infinitely steep slope and this is what was done in the previous section. There are two anomalies inherent in this approximation: the appearance of precursory waves at the beginning of the output signal resulting from the assumed ideal filter (infinite slope, zero phase shift), and Gibbs' phenomenon (ripple) on the envelope of the output signal. However, when the filter bandwidth is less than $\frac{2}{NT}$, where N and T are the number and the period of the cycles in the tone burst, no Gibbs' phenomenon occurs. This is the case for $N \leq 8$ for the equipment used in this experiment, so it is a good approximation for the signals of interest here.

The use of filters in the experiment described by the block diagram in Figure 7 has several advantages in addition to their primary function. For the input filter, these include:

1) The signal is less destructive to the driver. In this case, the driver is rated at 40 watts electrical drive, but with this signal we are able to drive it with 400-watt peak power pulses without damage. The driver diaphragm assemblies do not break until peak powers approaching 600 watts are applied, and even at this level breakage is caused simply from diaphragm or compliance rupture rather than from voice coil heating at pulse repetition rates of approximately 20 Hz. In fact, at frequencies above approximately 1 kHz, the sound level is limited by the power amplifier capabilities (a 260-watt audio frequency amplifier) rather than by driver limitations.

2) The requirement on the driver and power amplifier frequency response capability is reduced to merely one-sixth octave above the highest test frequency. If an unfiltered tone burst were used instead, the pulse characteristic would begin to change at the higher frequencies as the system upper frequency response capability began to be exceeded by the higher frequencies present in such a signal.

3) All the power dissipated by the driver and amplifier is concentrated near the test frequency, maximizing the total pulse power that is available to evaluate the material absorption.

The advantage of using a filter on the output include:

1) The signal-to-noise ratio of the signal is improved. Ambient room noise, microphone, and microphone amplifier noise set the limit on signal resolution when a differential comparator oscilloscope plug-in is used, as mentioned earlier. Hence, the improvement in signal-to-noise afforded by use of an output filter becomes significant.

2) At the high drive levels used for measurements at high-sound levels, power amplifier and driver distortion becomes noticeable. The output filter removes these distortion components.

Oscilloscope photographs of the signal just described are shown in Figure 13. In Figure 13-a, the tone-burst generator output for N = 8 is shown. The resulting filter output is shown in Figure 13-b. The time axes in these photographs are all identical, but the amplitude scales have been adjusted to approximately equal excursion on the oscilloscope. The driver output without filters in the system is shown in Figure 13-c, and the same signal with the input filter in is shown in Figure 13-d.

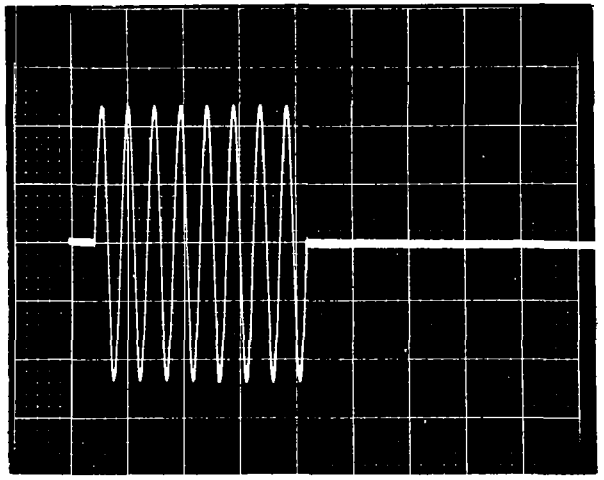

a. TONE BURST GENERATOR OUTPUT

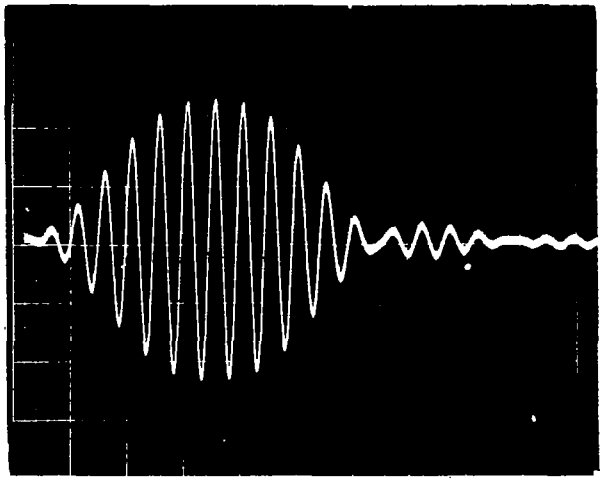

b. FILTERED TONE BURST (ONE-THIRD OCTAVE FILTER)

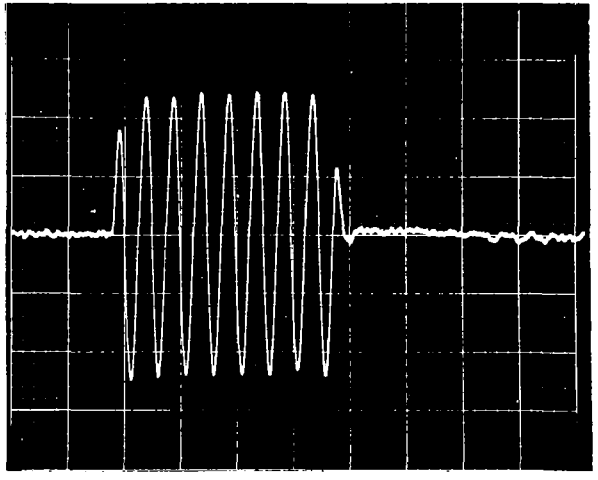

c. DRIVER OUTPUT WITH UNFILTERED TONE BURST INPUT

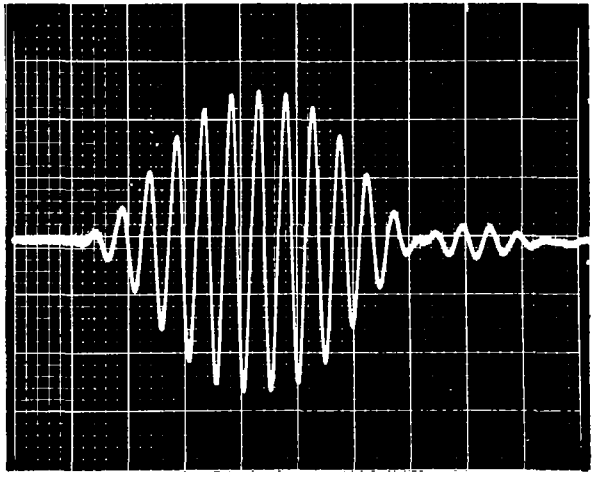

d. DRIVER OUTPUT WITH FILTERED TONE BURST INPUT. (ONE-THIRD OCTAVE FILTER)

FIG. 13. TONE BURST INPUT SIGNAL AFTER VARIOUS STAGES OF PROCESSING. 1K Hz CENTER FREQUENCY, 8 CYCLE DURATION.

Typical incident and reflected tone bursts (for the empty tube) are shown in Figure 14. In a), the signal with no filtering in the system is shown. Figure 14-b through 14-d show the signal with various degrees of filtering. The slow rise and fall resulting from the filter is apparent. Also note the lower noise level in c) and d) compared with b). This noise reduction becomes significant when the signals are highly amplified by the differential comparator plug-in. The signals actually read by this technique are shown in Figure 15, from which it is apparent that with this degree of magnification even relatively small noise levels can reduce the readout accuracy; hence, one reason for the output filter.

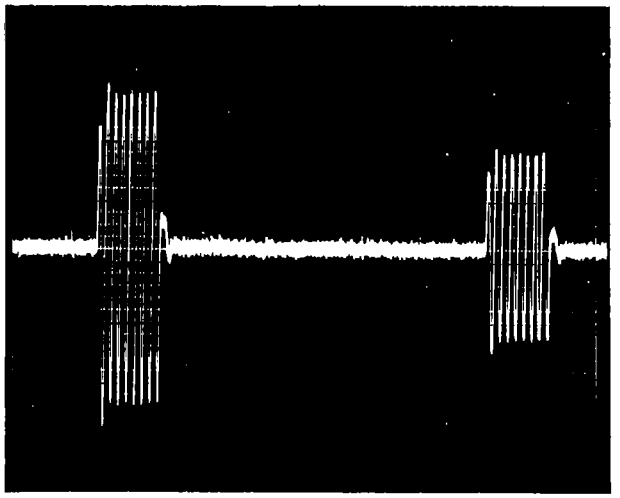

a. No Filtering

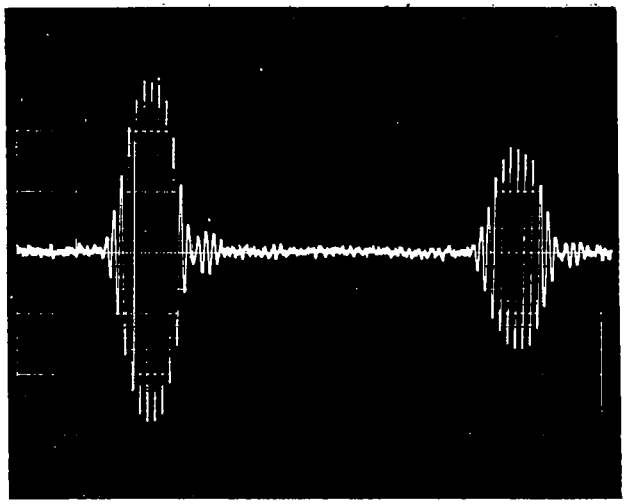

b. Driver input only Filtered

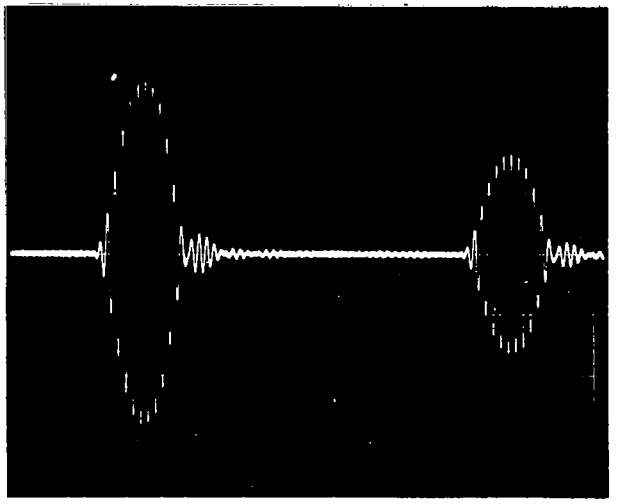

c. Microphone output only Filtered

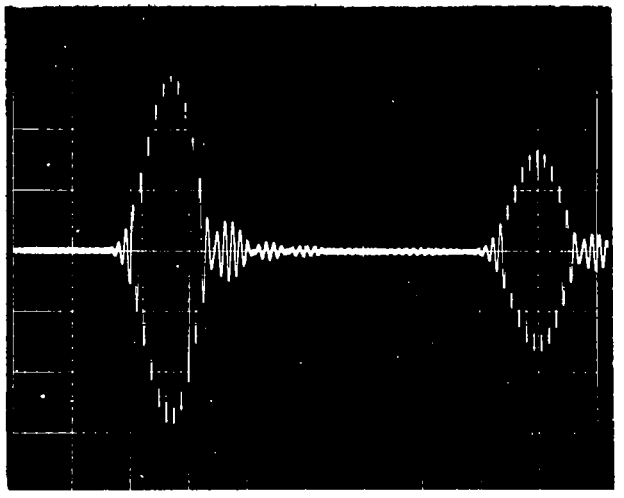

d. Both driver input and microphone output Filtered

FIG. 14. CHARACTERISTICS OF THE INCIDENT AND REFLECTED TONE BURST WITH VARIOUS DEGREES OF SIGNAL FILTERING

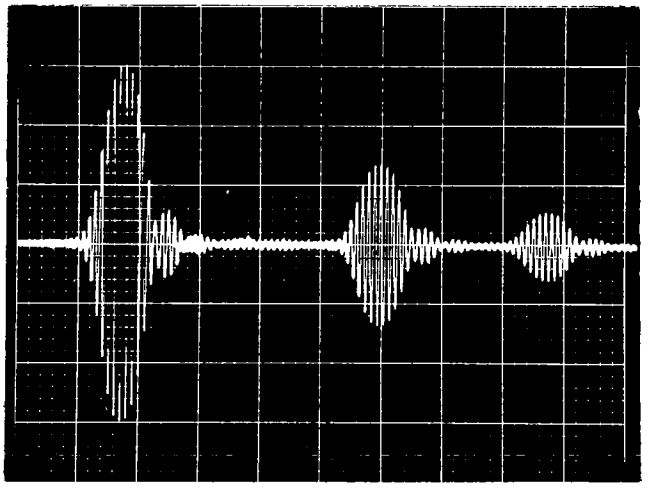

a. 8 cycle tone burst. The large pulse is the incident signal, the center pulse is the reflection from the sample, and the last pulse in the reflection from the driver.

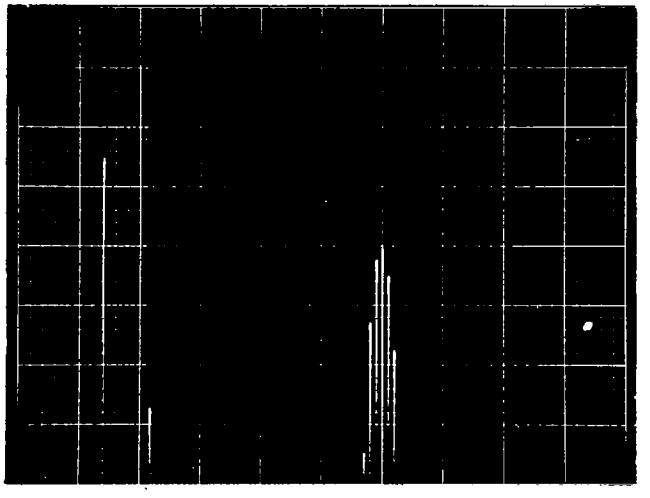

b. This is the signal shown in Figure a) but with the oscilloscope vertical sensitivity increased by a factor of 10 and an offset applied with the differential comparator to read the peak amplitude of the reflection from the sample. With this magnification the incident pulse is off-scale.

FIG. 15. USE OF THE DIFFERENTIAL COMPARATOR TO READ PULSE HEIGHT

Application of the Technique

The procedure just described was used to obtain low intensity (i.e., in the linear region) absorption coefficient data on polyurethane foam, fiberglass, polyurethane foam with one-inch thick honeycomb backing, fiber metal with one-inch thick honeycomb backing, and sintered bronze on honeycomb. Similar data were obtained by the standard impedance tube technique for comparison. These data are presented in Figures 16 through 21. The agreement between the two methods of measurement is excellent and demonstrates the general characteristics one would expect from each type of absorber. (See refs. 1 to 5 and 7.) The data extends nearly an octave above the upper limit of the impedance tube. There would be no inherent difficulty in extending the upper frequency limit considerably farther, other than the fact that the tube losses and driver limitations would tend to reduce the maximum PPL. For the purpose of this program, it is felt that 10 kHz is a reasonable upper frequency limit.

The absorption coefficient of the three resonant absorbers (resistive material on honeycomb) was determined as a function of PPL to measure anticipated nonlinearities. The results of these measurements are shown in Figures 21, 22, and 23. It is seen that the fiber metal and sintered metal samples become quite level dependent above 140 dB PPL at frequencies above 1 kHz, while the foam remains quite linear to 6 kHz. In Figures 21 and 23, the 163 dB PPL curve extends only to 3 kHz because tube dimensions were not optimized and the power amplifier was not capable of driving the transducer to its peak capacity.

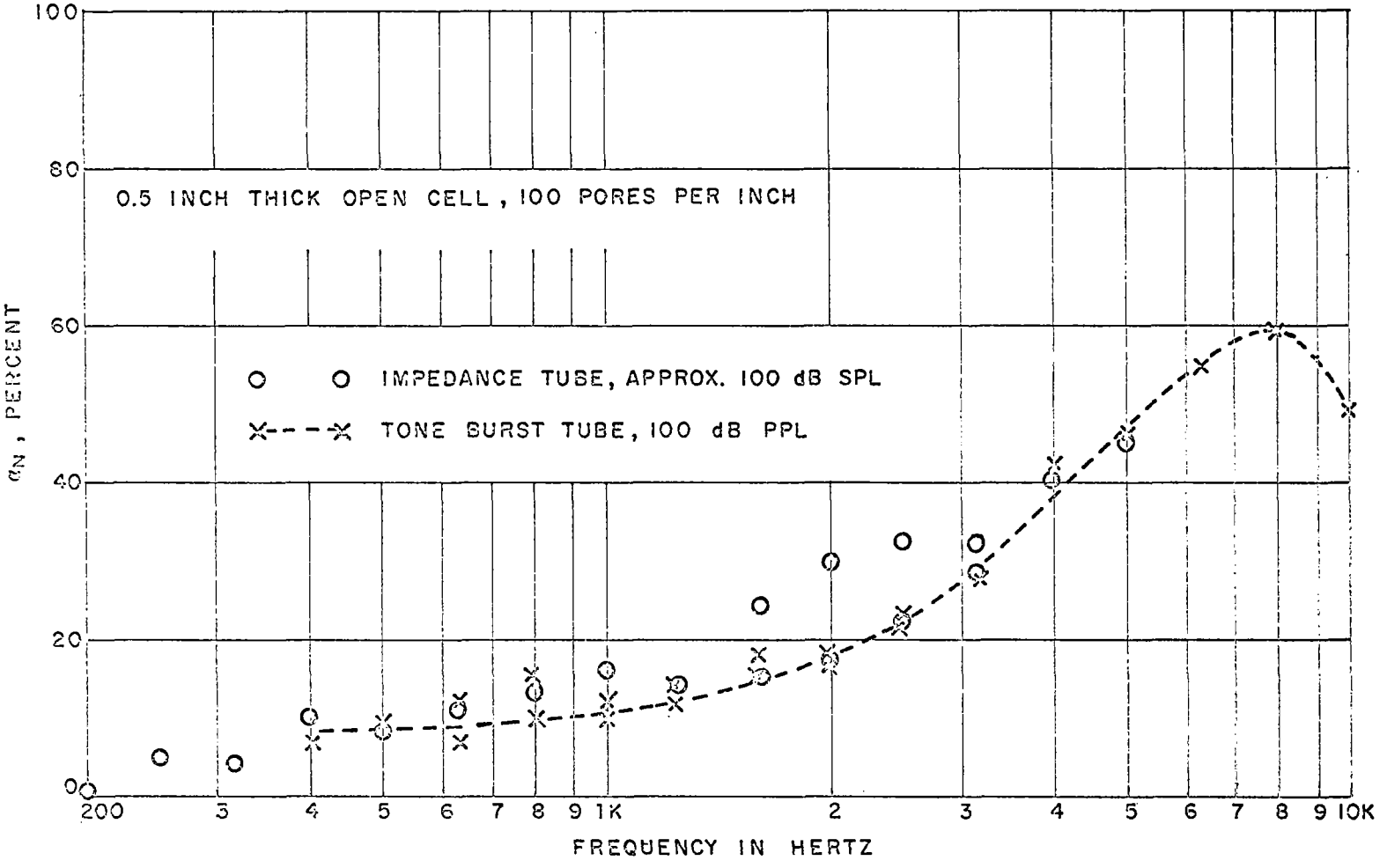

FIG. 16. ABSORPTION COEFFICIENT – POLYURETHANE FOAM WITH RIGID BACKING. COMPARISON OF IMPEDANCE TUBE AND TONE BURST TUBE DATA

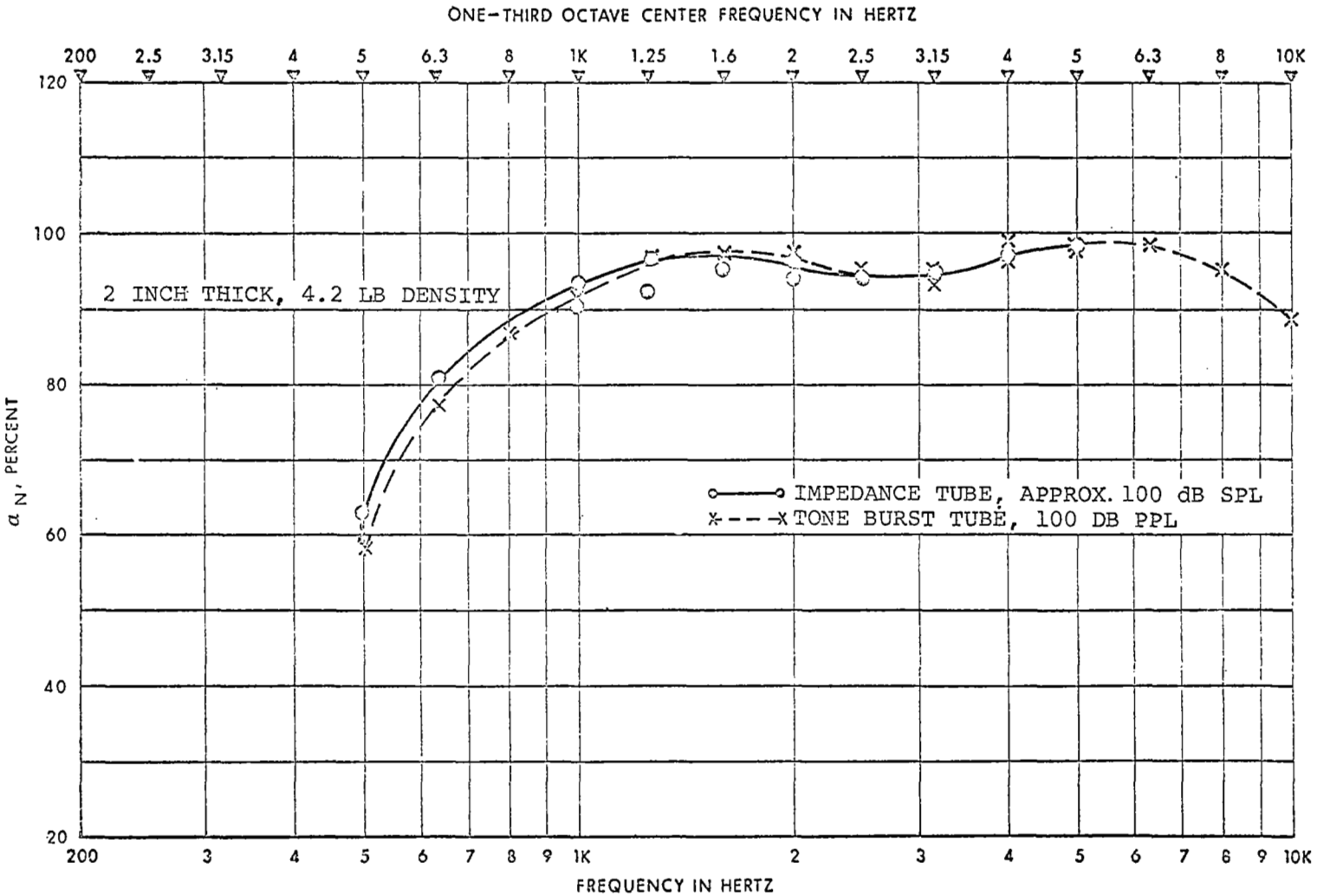

FIG. 17 ABSORPTION COEFFICIENT-FIBERGLASS
COMPARISON OF IMPEDANCE TUBE AND TONE BURST TUBE DATA

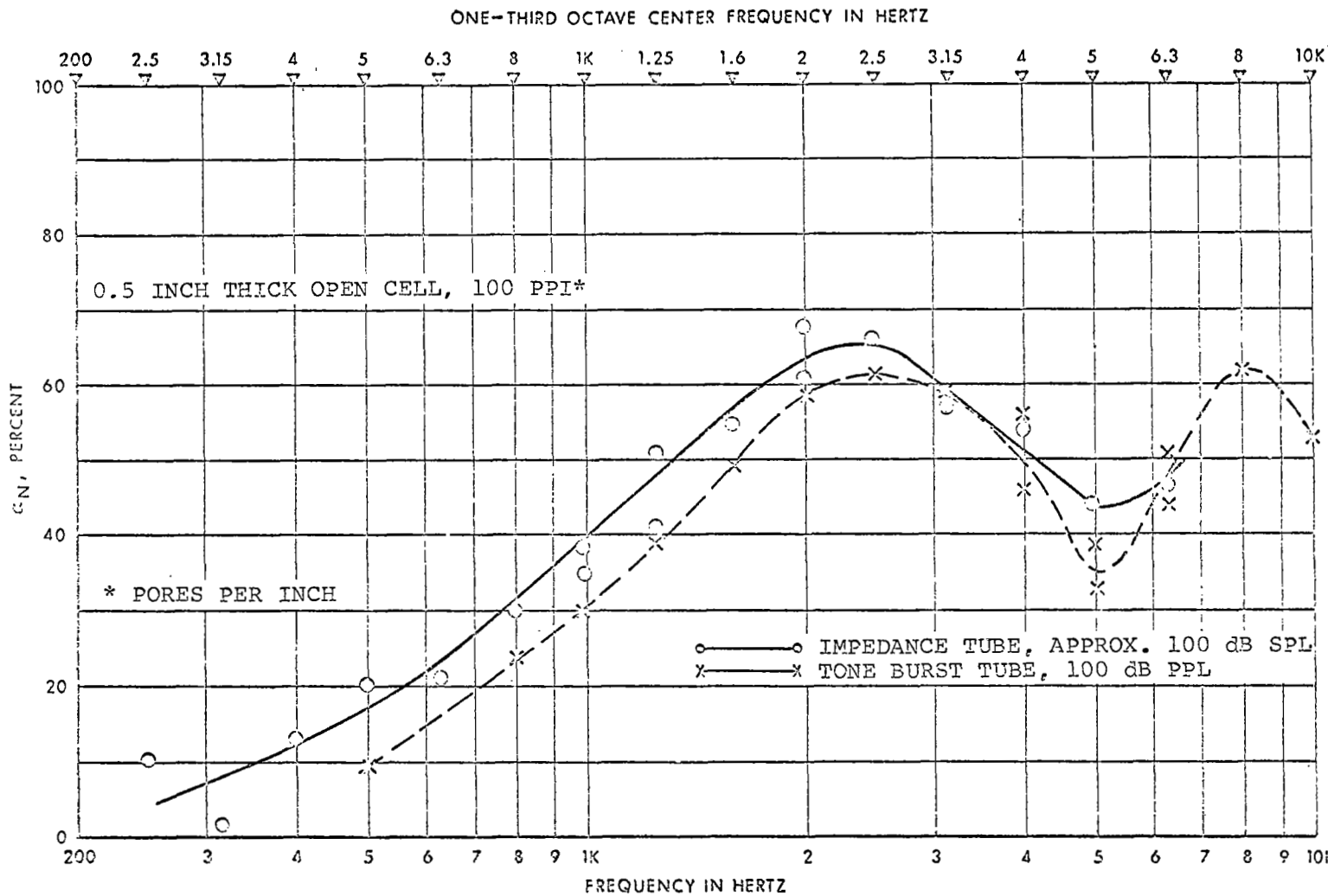

FIG. 18 ABSORPTION COEFFICIENT-POLYURETHANE FOAM ON 1 INCH HONEYCOMB
COMPARISON OF IMPEDANCE TUBE AND TONE BURST TUBE DATA

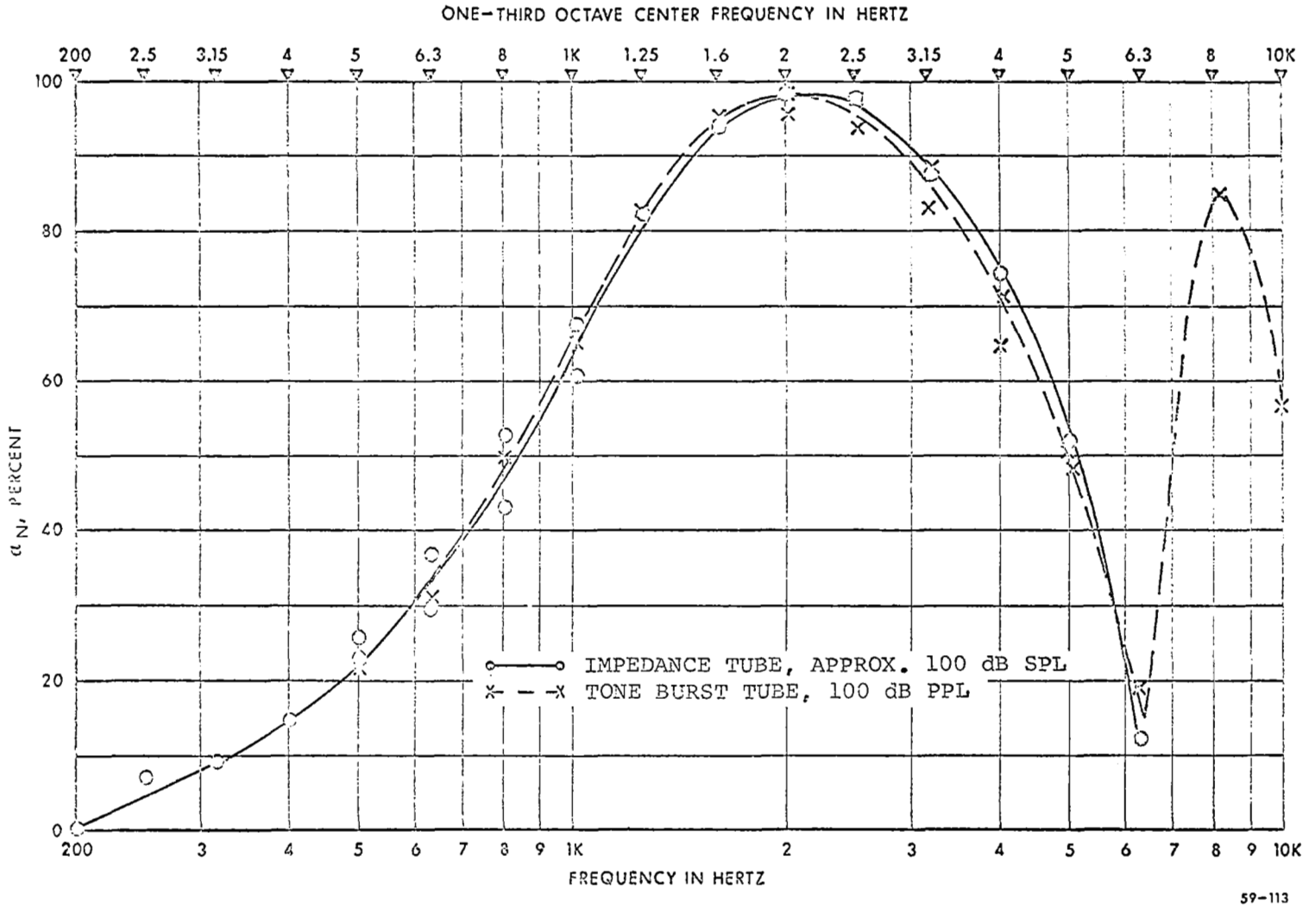

FIG. 19 ABSORPTION COEFFICIENT-50 RAYL FIBERMETAL ON 1 INCH HONEYCOMB COMPARISON IMPEDANCE TUBE AND TONE BURST TUBE DATA

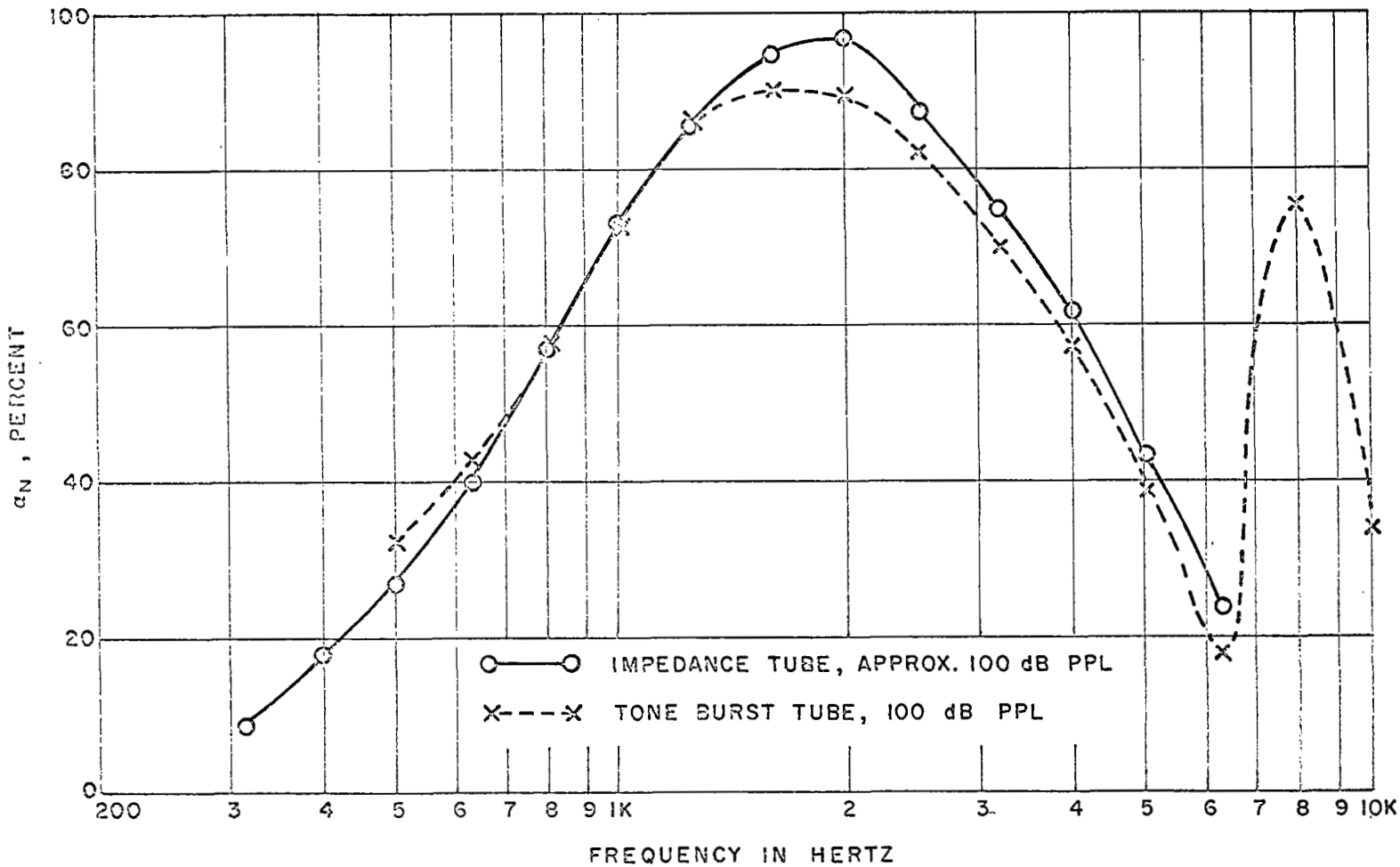

FIG. 20. ABSORPTION COEFFICIENT – 120 RAYL SINTERED BRONZE ON 1 INCH HONEYCOMB. COMPARISON OF IMPEDANCE TUBE AND TONE BURST TUBE DATA

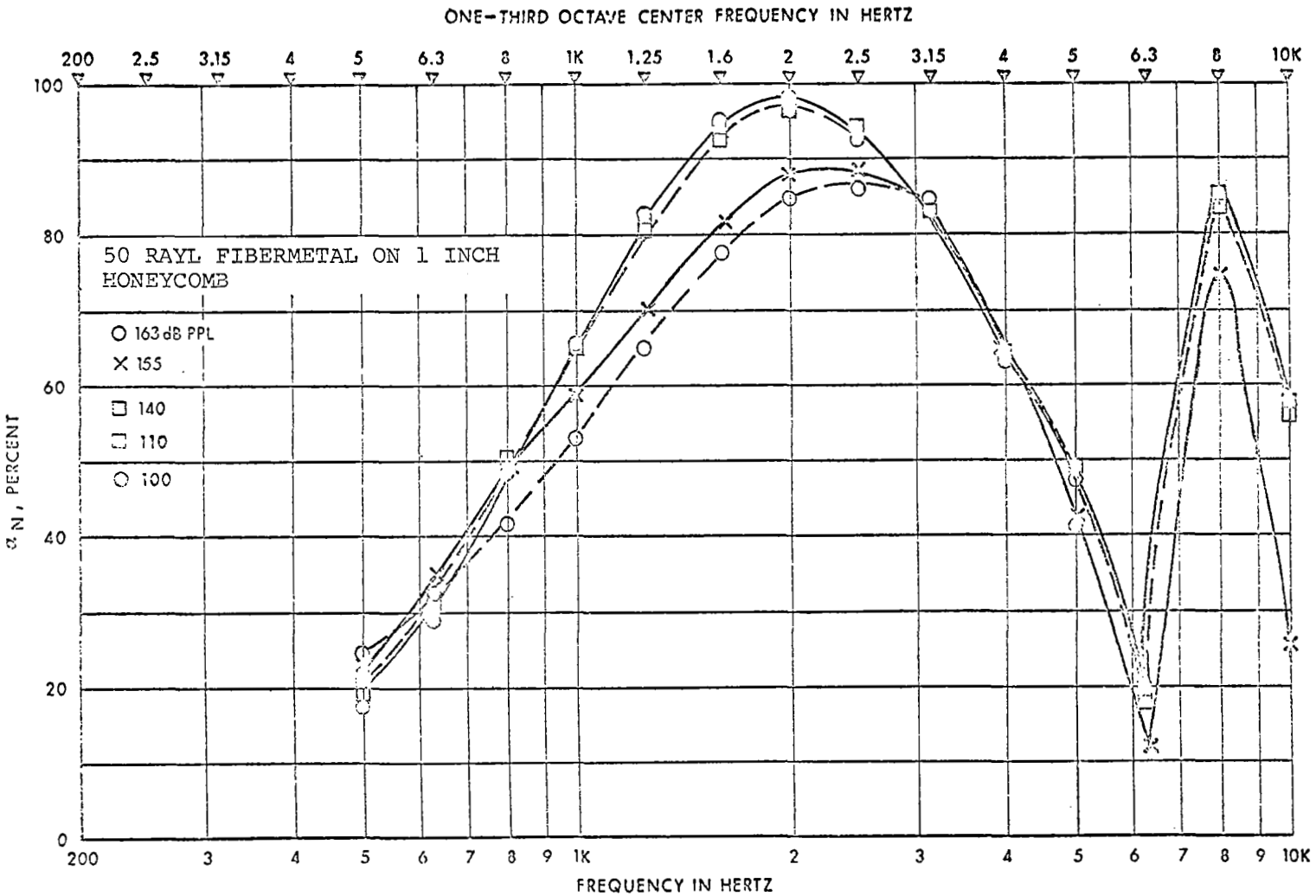

FIG. 21 VARIATION OF ABSORPTION COEFFICIENT WITH SOUND INTENSITY

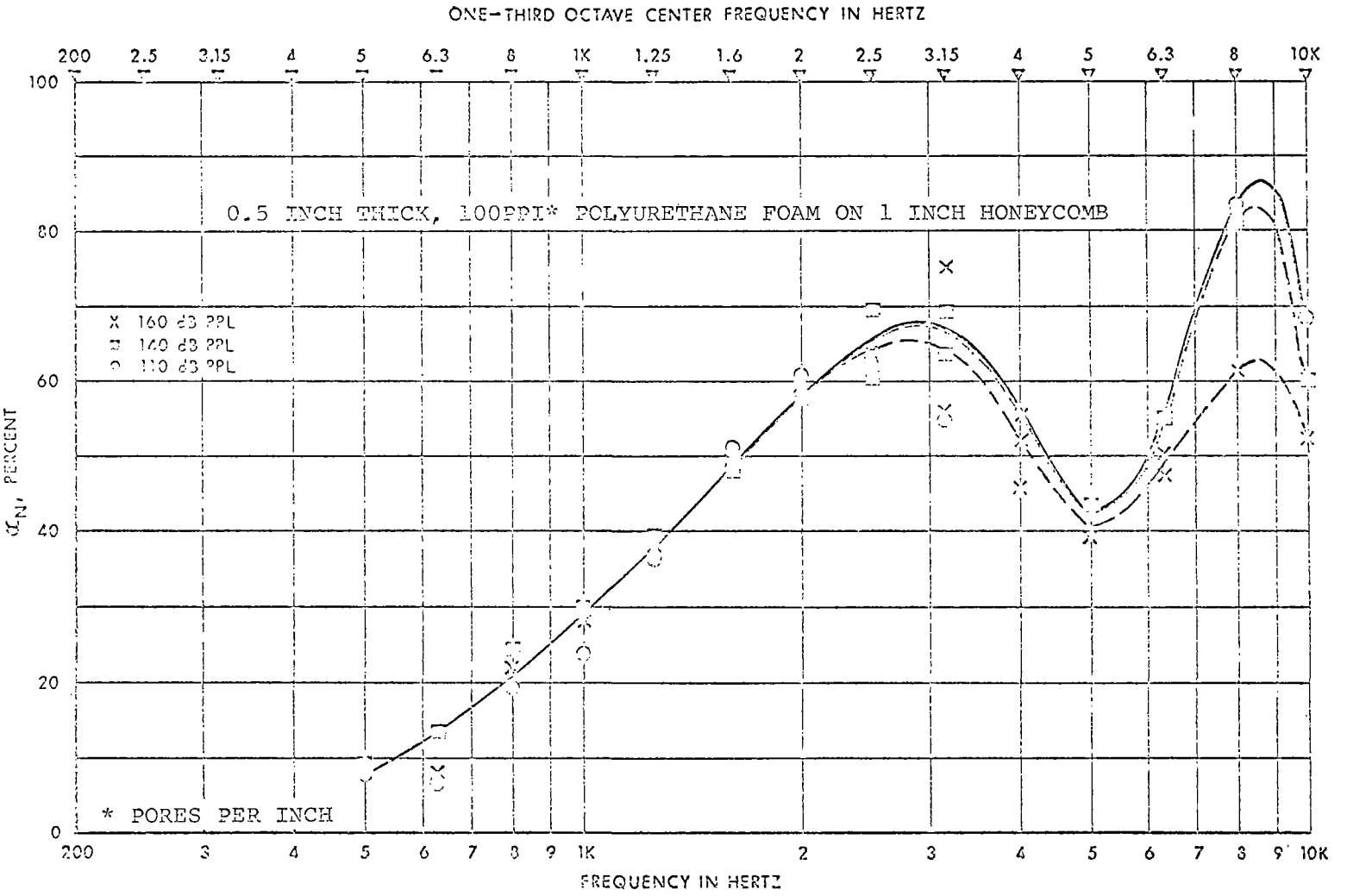

FIG. 22 VARIATION OF ABSORPTION COEFFICIENT WITH SOUND INTENSITY

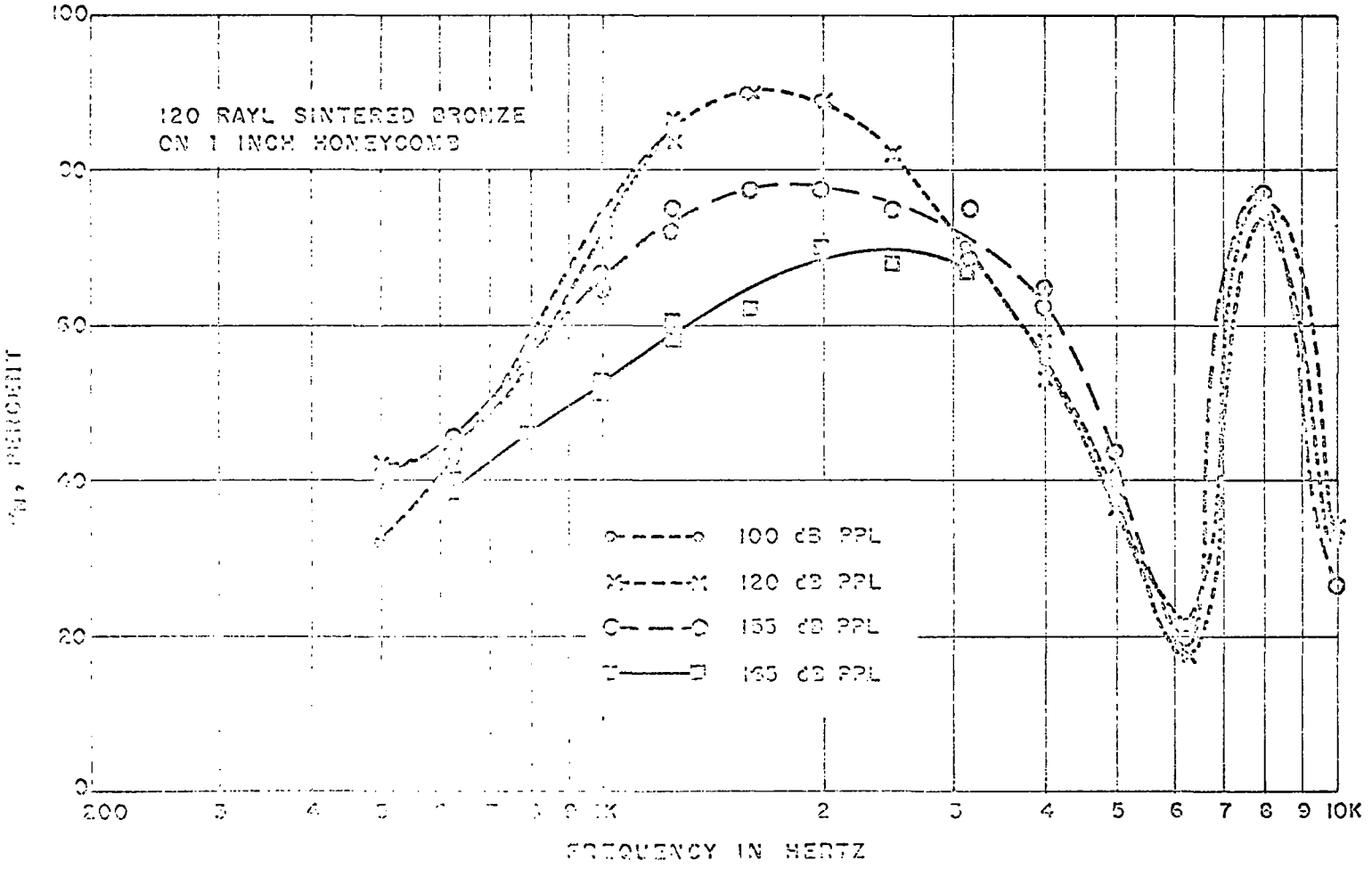

FIG. 23. VARIATION OF ABSORPTION COEFFICIENT WITH SOUND INTENSITY

SHOCK TUBE MEASUREMENTS

General Description of the Technique

The shock tube used in this program is simply a tube of uniform diameter in which a diaphragm initially separates two sections at different pressures. Bursting of the diaphragm generates a flow containing waves of finite amplitude. The shock wave thus produced can be used to measure the absorption of high-intensity sound by samples of acoustic absorbers.

A block diagram of this basic experimental apparatus is shown in Figure 24. The shock tube and pneumatic control console are shown in Figure 25. The 3-inch I. D. tube is 17 feet long overall, with a 5-foot long driver section. Pressure sensors are located at any of several stations located along the length of the tube. A movable piston in the sample holder is used to locate the sample surface or rigid piston face at the same location for all measurements. The sensor outputs are passed through spectrometers, which contain amplifiers and one-third octave filters, to obtain absorption data as a function of frequency. Normally, only one sensor is used, but two are shown in Figure 24, and two sensors have been used to obtain propagation loss information.

Referring to Figure 24, the sequence of events during shock tube operation proceeds as follows. Air is admitted until the driver section is at the desired pressure. This pressure determines the shock strength and thus the sound

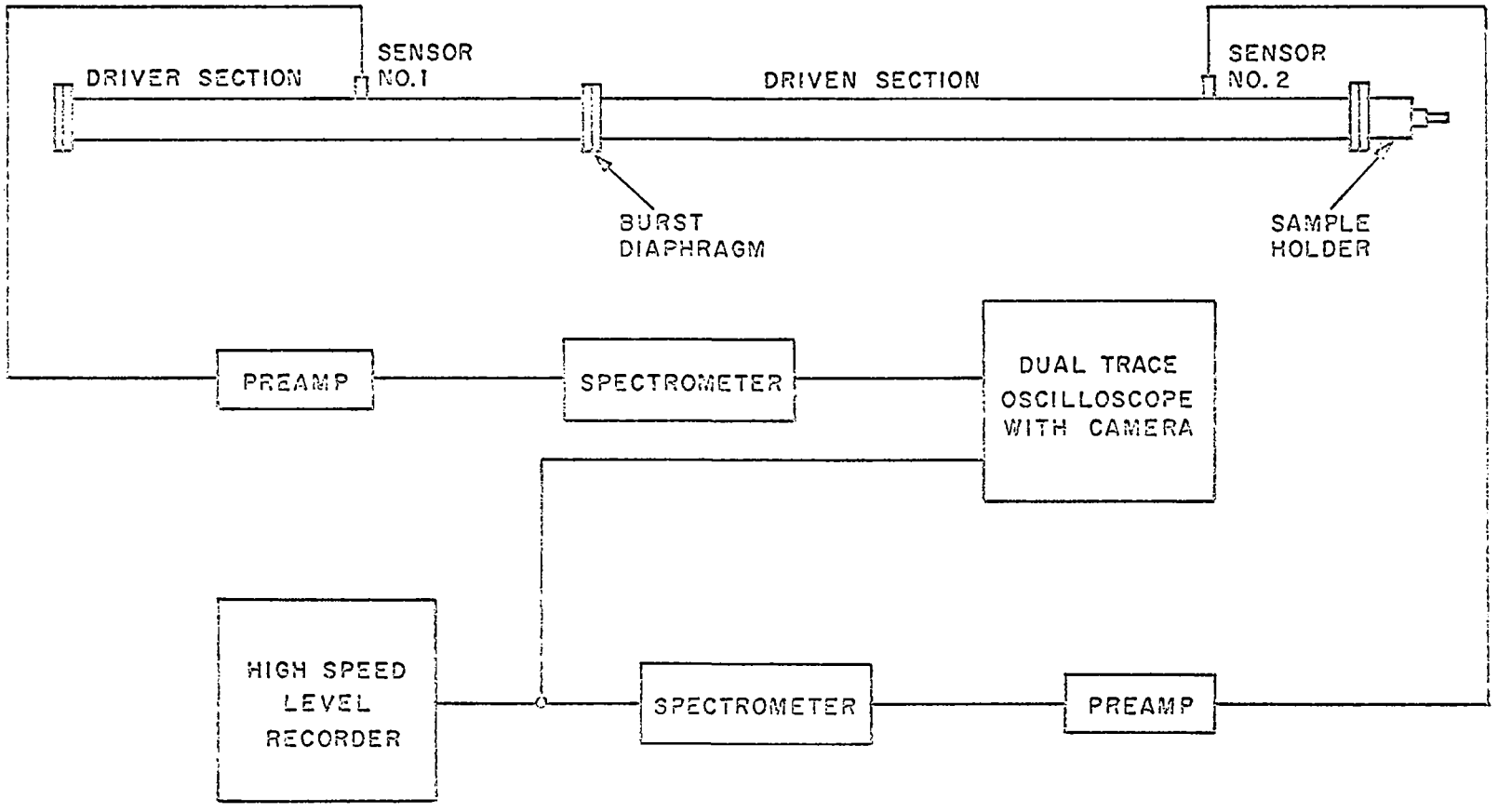

FIG. 24. GENERALIZED BLOCK DIAGRAM - SHOCK TUBE ABSORPTION MEASUREMENT

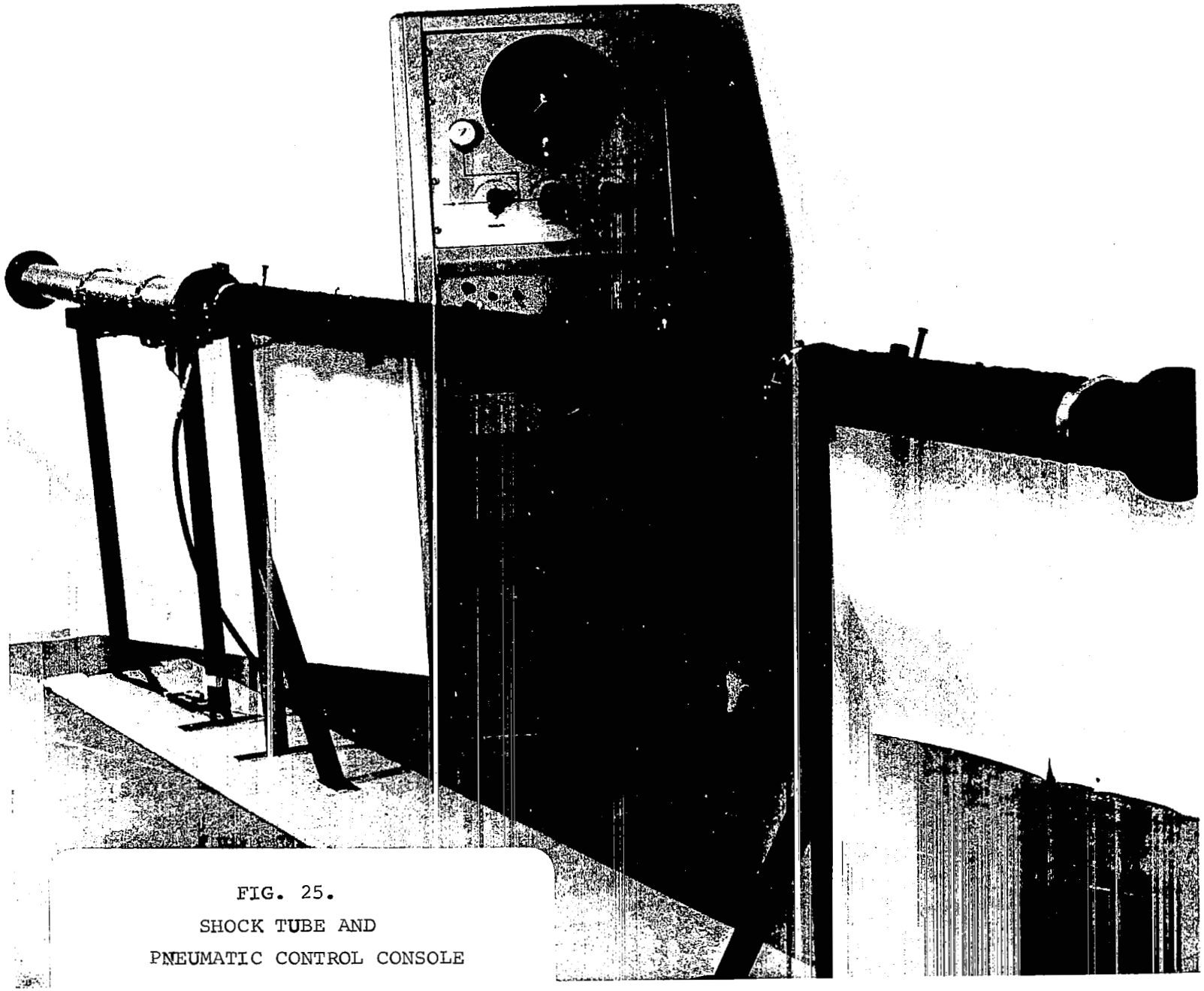

FIG. 25.
SHOCK TUBE AND
PNEUMATIC CONTROL CONSOLE

output (references 8 and 9). When the burst diaphragm is broken by an electrody mically actuated plunger, a shock wave propagates down the driver section of the tube (at nearly sonic velocity for pressure ratios of interest in this study) toward the solid or sample surface. Simultaneously, a rarefaction wave propagates back through the driver section. These waves are reflected from the ends of the tube and propagate in the opposite direction, where they are again reflected from the tube ends, and so on. The quasi-steady flow regions induced behind these waves upon diaphragm rupture are separated by the gas "piston" created by this rupture. This interface is called the contact surface. Pressure and particle velocity are constant across this surface, but temperature and density change abruptly.

The wave system in the tube is shown in the characteristic diagram of Figure 26. In preparing this diagram, the velocity of the various waves is calculated by using well known shock tube relations (reference 9). These velocities are considered accurate only to the first interaction of the waves. With the exception of the initial driver section pressure P_4, wave pressures are normally expressed as a ratio P_{ij}, where:

$$P_{ij} = \frac{\text{Pressure in region (i)}}{\text{Pressure in region (j)}} \qquad (9)$$

Thus, the pressure jump across the incident shock wave is P_{21}, while that across the reflected shock is P_{52}.

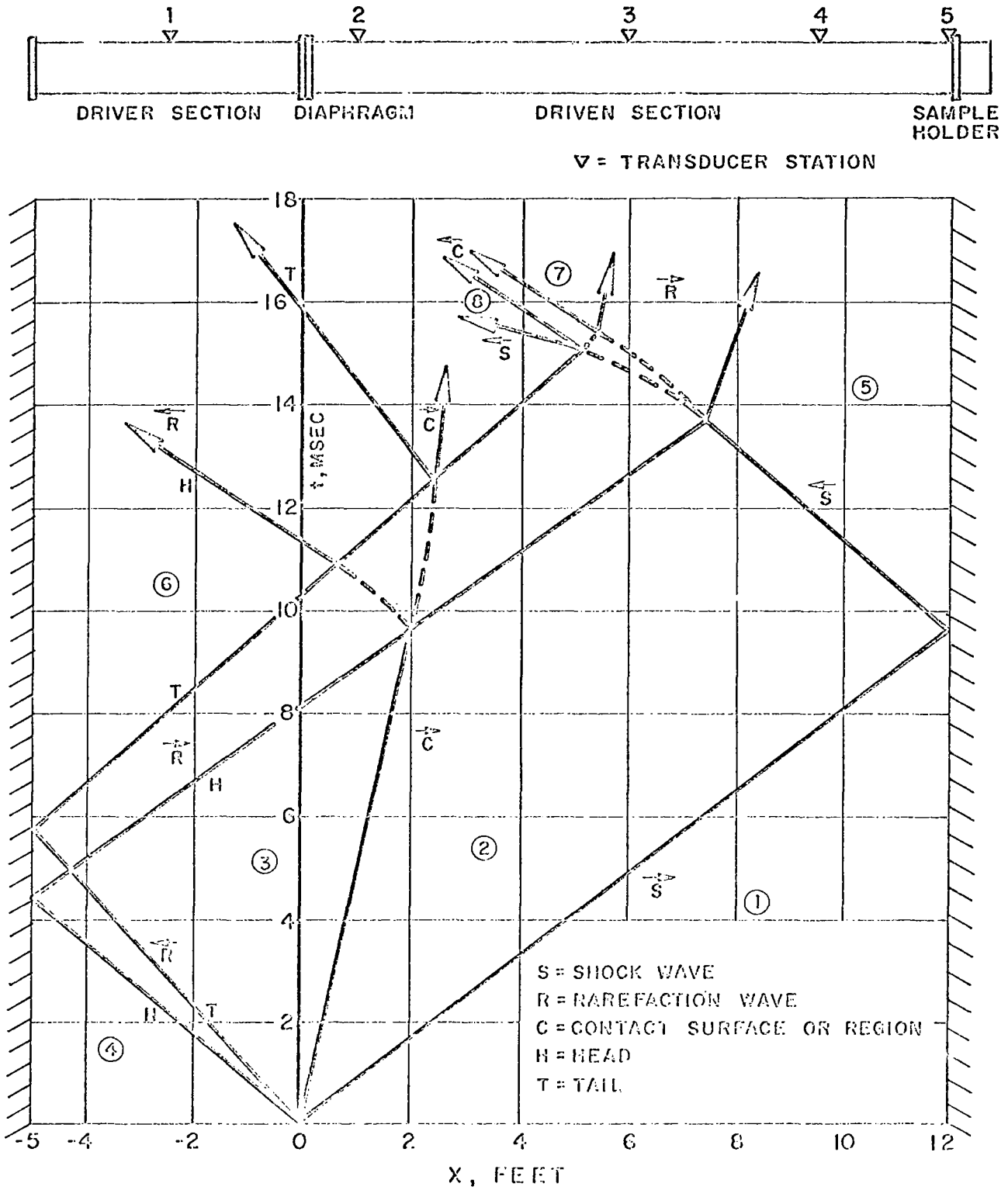

FIG. 26 WAVE SYSTEM IN THE SHOCK TUBE FOR A RIGID TERMINATION

Much of the work in the shock tube has been performed at a driver section pressure P_4 of 10.4 PSIG, a convenient pressure for which several shock tube parameters have been tabulated (ref. 8). For a P_4 of 10.4 PSIG, we have for the various pressure ratios shown in the diagram:

$$P_{41} = 1.68$$

$$P_{21} = 1.3$$

$$P_{52} = 1.3$$

$$P_{32} = 1$$

$$P_{34} = P_{24} = .76$$

$$P_{54} = 1.8$$

From the diagram it is apparent that an exceedingly complex wave system obtains in the tube after only a very few reflections of the primary shock wave. This situation would seem to preclude a precise analytical description of conditions within the tube at any given time, and to favor a statistical approach.

The output from the first sensor during the sequence of events following diaphragm rupture is shown in Figure 27. The first peak, of pressure P_a, is the initial passage of the primary shock wave; the second output pulse, of pressure P_b, is the primary shock after reflection from the driven section end (either a solid end plate or a material sample); the third pulse of pressure P_c, is the rarefaction wave passing the sensor after reflection from the driver end of the shock tube; and so on.

Each successive shock wave is reduced in amplitude from the previous one by an amount corresponding to the loss due to: a) tube walls, air loss, reflection or scattering from the

rarefaction wave, etc., and b) reflection from the solid end plate or from the test sample.

Ideally the pressure would remain constant between the arrival of the incident shock of pressure amplitude P_a and the arrival of the reflected shock of amplitude $P_b - P_a$ at the pressure sensor of Figure 27. The apparent loss in pressure shown in the figure during the time interval between these two events is caused by the low frequency roll-off of the pressure sensor and electronics.

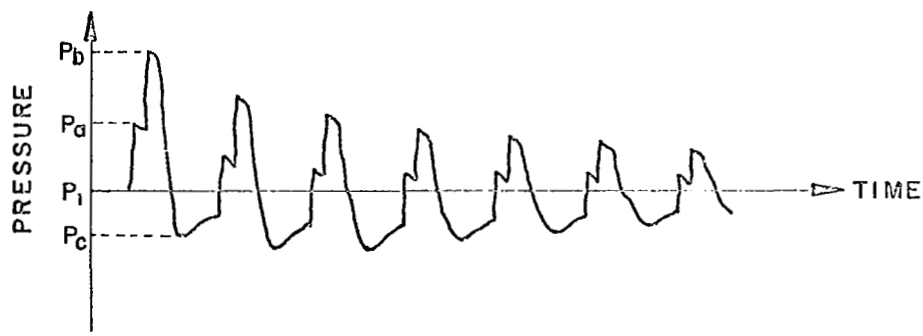

FIGURE 27. OUTPUT FROM SENSOR NO. 2 OF FIGURE 24

The primary goal of this portion of the program was to determine the practicability of using a shock tube to measure the sound absorption characteristics of materials at high intensities. One method of doing this would be to treat the shock tube as a one-dimensional reverberation chamber. Such a notion has several appealing features.

One is the fact that the sound field could be considered a single wave reflecting back and forth along the tube. This would eliminate or reduce such troublesome considerations common to three dimensional reverberation chambers as the randomness of the sound field, modal density, and distribution. (See refs. 10 and 13.) Other potential advantages would include the portability of the apparatus, the fact that the output from only one transducer need be evaluated, and the exceptionally wide range of frequencies that are available in the signal.

As described previously, an exceedingly complex wave system occurs in the tube after only a very few reflections of the primary shock wave. This situation would seem to favor such a reverberation time, or decay rate, technique of absorption measurement, since after a short period of time the interactions of the waves would become so frequent that they could be considered continuous from a macroscopic point of view. The resultant variations in the shock strength could therefore be lumped into one propagation loss term. The measurement of absorption would therefore only involve a measurement of the shock strength decay rate or reverberation time. However, as will be discussed in a later section, other considerations were found to completely negate these potential advantages.

Another possible approach is to treat the shock wave as a normally incident acoustic pulse, and determine the absorption from the ratio of the reflected to the incident

pulse amplitude. In principle, this method would be expected to result in greater data scatter than the reverberation technique due to the many perturbations experienced by any given wave traversing a length of the tube. In practice, it can be made to yield more accurate results, although only with experimentally difficult technique.

A third approach, which is an extension of the above technique, would be to expand the shock to weaken it. Such an approach would reduce any deleterious effects resulting from the large pressure jump in the normal shock tube, which is at least partially responsible for the deficiencies of the other two methods. Thus, expanding the shock and treating it like an acoustic pulse would help bridge the gap in intensity between conventional measurement techniques and the shock tube method. An apparatus designed to accomplish this is shown in Figure 28. The shock tube cross-sectional area is exponentially increased by a factor of 20 in the transition section, resulting in a reduction in acoustic pressure of 13 dB. This approach has shown considerable promise, but the program was concluded before definitive experiments could be performed.

Theoretical Considerations

Where small signal theory is applicable, the reflection coefficient* of a smooth, rigid, impermeable surface is

* Throughout this report, unless otherwise stated, the term "reflection coefficient," denoted by R, is to be taken as the energy reflection coefficient, equal to $1-\alpha$. This term is used in the derivations rather than α for the sake of brevity. A lower case r is used for the pressure reflection coefficient.

inviolably taken as less than or equal to unity. This condition no longer holds in a shock tube, however, where reflection coefficients greater than unity have been measured with the experimental arrangement of Figure 24. Such a situation does not violate the conservation of energy, of course, but merely means that some energy has been transferred to the spectral band being measured from some other spectral region during the time interval between the measurement of the incident and the reflected pulse amplitude. This situation does, however, present some problems when formulating an expression for the absorption coefficient. Linear formulations contain the constraint, either implicitly or explicitly, that the reflection coefficient for any surface be equal to or less than unity. This does not necessarily hold for finite amplitude waves.

One way of circumventing this situation is to set the absorption of the sample equal to the reduction in amplitude of the reflected shock with the sample terminating the tube compared to its amplitude reduction with a rigid termination.

In other words, we will say that the reflection coefficient of a sample measured by the pressure sensor is a function of both the actual reflection coefficient of the sample and the reflection coefficient of a rigid termination at that particular frequency and incident shock strength. Stating this mathematically,

$$R_2 = f(R_s)g(R_1) \qquad (10)$$

where R_2 = the measured reflection coefficient of the sample

$f(R_s)$ = an arbitrary function of the actual reflection coefficient of the sample

$g(R_1)$ = an arbitrary function of the reflection coefficient of the rigid termination

The functional relationship between these terms can be determined explicitly by applying the following three conditions. First, if $R_s=0$ (that is, $\alpha_s=100\%$), then we must have $R_2=0$, since if the sample absorbs all the incident energy, then by definition there is no reflection. That is,

$$\text{i) for} \qquad R_s=0,\ R_2=0,$$

$$\text{or} \qquad 0=f(0)g(R_1)$$

For a non-trivial solution, $f(0)=0$, so that $f(R_s)$ can be set equal to an arbitrary polynomial:

$$f(R_s) = AR_s + BR_s^2 + CR_s^3 + \ldots \tag{11}$$

where the first, or constant, term must be zero.

Next, if $R_s=1$, then by definition the sample appears identical to the rigid termination and reflects all the incident energy. Therefore,

$$\text{ii) for} \qquad R_s=1,\ R_2=R_1$$

$$\text{or, from (10) and (11),}$$

$$R_2=R_1=f(1)g(R_1)=(A + B + C + \ldots)g(R_1) \tag{12}$$

As a third condition, any relationship of the form (10) must converge to $R_2=R_s$ in the low intensity limit. In this limit,

$$\text{iii)} \quad R_1=1 \text{ and } R_2=R_s,$$

$$\text{or} \quad R_2=R_s=f(R_s)g(1) = (AR_s+BR_s^2+CR_s^3+\ldots)g(1),$$

from which $B=C=D\ldots=0$. Therefore (12) becomes

$$R_1=Ag(R_1), \tag{13}$$

from which $A=1$, since A is constant and independent of R_1. If $A=1$, then (13) becomes

$$g(R_1) = R_1$$

Substituting these results into (11),

$$f(R_s) = R_s$$

Therefore, (10) becomes $R_2=R_sR_1$, or

$$R_s = \frac{R_2}{R_1} \tag{14}$$

which simply states that we are using the actual value of the reflection coefficient of a rigid surface as a basis for determining R_s, rather than an arbitrarily assigned value of unity.

In an effort to circumvent the nonlinearities encountered with the shock tube reverberation and the shock reflection techniques, a preliminary investigation was performed with an expanded shock.

It has been shown that the wave system is extremely complex after the first reflection and this is more so for the expansion tube. This precludes the use of any data reduction technique other than amplitude reduction of the initial shock. Equation (14) is employed with the aid of which it can easily be shown (see the section on the tone burst tube) that the pressure reflection coefficient is given by

$$r_s = \frac{P_{rs}}{P_{ro}} \qquad (15)$$

where P_{rs} = reflected PPL with a sample termination

P_{ro} = reflected PPL with a rigid termination

when the incident PPL's are equal.

Another possible method of determining the absorption coefficient of a sample of absorptive material with the shock tube is by measuring the ratio of reflected to incident shock pressure jump as recorded with an oscilloscope camera for the basic, constant area shock tube. The entire process of shock energy decay can be recorded and analyzed in this manner by successively increasing the time delay between diaphragm rupture and oscilloscope triggering. Each successive reflection from the sample surface could then be analyzed to calculate the absorption coefficient from Equation (15).

The initial concept was to treat the shock tube as a one-dimensional reverberation chamber. Following this line of thought, an expression for R_s in terms of the reverberation time can be derived with the aid of Equation (14). Referring to the following diagram, we

assume that the shock wave reflects back and forth in the tube until the energy is dissipated, and treat the shock tube as a one-dimensional reverberation chamber, with sample absorption of energy occurring at discrete time invervals rather than continuously. Keeping in mind the wave diagram of Figure 26, it is apparent that interaction of the shock wave with other waves may appear as a transmission loss term along with wall losses. These losses will be treated as continuous throughout the length of the tube and lumped into one propagation loss term per transit.

This propagation loss, denoted by β, is defined by the relation

$$\epsilon = \epsilon_o e^{-\beta x}$$

where ϵ_o is the initial energy in the shock wave and ϵ is the energy remaining after the shock has traveled x feet down the tube with no intervening reflections from a tube end.

Beginning with diaphragm rupture, the energy is dissipated as shown in the diagram below. End (A) can be terminated either with the sample of interest or with a rigid plate, while end (B) is always a rigid plate.

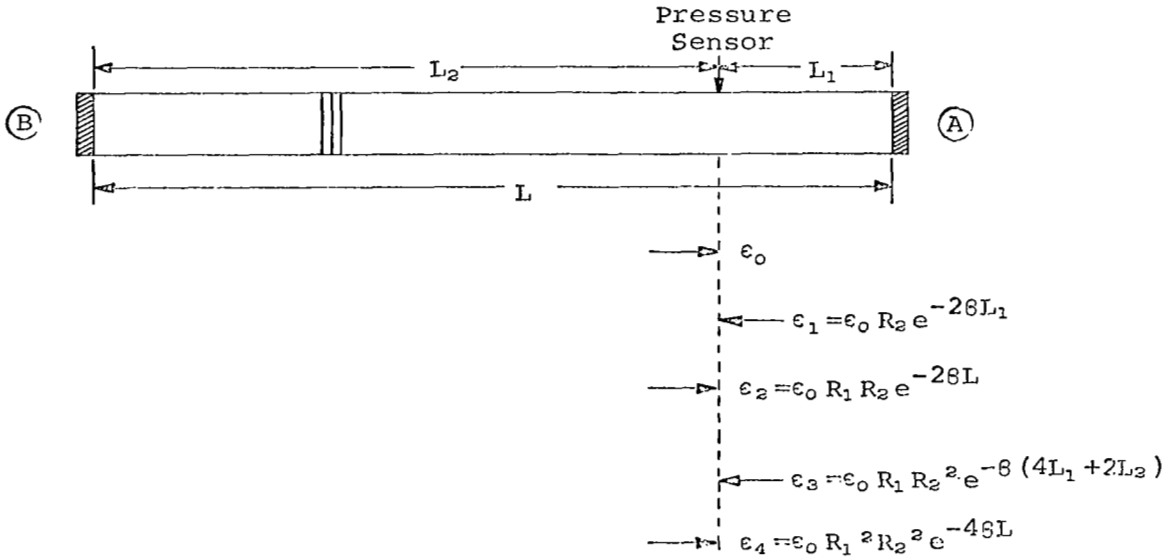

after n reflections, the energy is

$$\epsilon_n = \epsilon_o R_1^{\frac{n}{2}} R_2^{\frac{n}{2}} e^{-n\beta L} \qquad (16)$$

This expression is correct to better than one tube length of travel, which is a good approximation for large n. For a rigid termination at end (A), $R_2 = R_1$ and (16) becomes

$$\epsilon_n = \epsilon_o R_1^{n} e^{-n\beta L} \qquad (17)$$

Now $nL = ct$ where c is the propagation velocity (taken as the speed of sound for pressure ratios of interest here). Defining the reverberation time T_o as the time required for the energy to decay to one millionth its initial value,

$$\frac{\epsilon_n}{\epsilon_o} = 10^{-6} = R_1^{\frac{CT_o}{L}} e^{-\beta CT_o}$$

from which $$\beta L = \ln R_1 + \frac{13.8L}{CT_o} \qquad (18)$$

where ln is the natural logarithm.

For a sample termination at end (A), the same process yields

$$-13.8 = \frac{CT_s}{2L}\left(\ln R_1 + \ln R_2\right) - \beta CT_s$$

where T_s is the reverberation time with a sample. Substituting the value of βL from equation (18),

$$\ln R_2 - \ln R_1 = \frac{2 \times 13.8L}{c}\left(\frac{1}{T_s} - \frac{1}{T_o}\right)$$

Taking the natural logarithm of (14) gives $\ln R_2 - \ln R_1 = \ln R_s$, so that

$$R_s = \exp\left[\frac{-2x13.8L}{c}\left(\frac{1}{T_s} - \frac{1}{T_o}\right)\right] \qquad (19)$$

This equation yields values for the absorption coefficient which are much too low. In an attempt to resolve this difficulty a different formulation was tried. This alternate approach involves a different definition of shock strength, and is also more complex in the sense that a computer is required to obtain a numerical answer from the final equation. It is necessary to modify and expand the notation somewhat as shown in the diagram below.

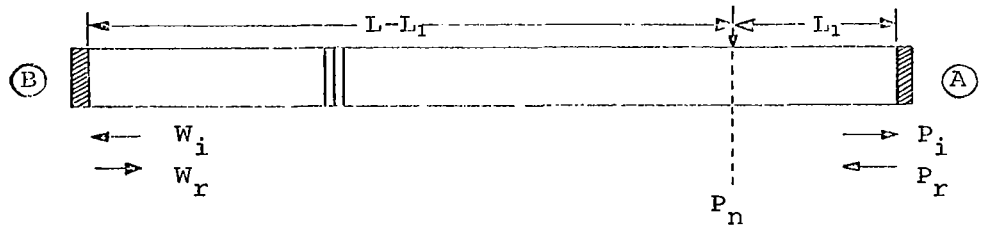

The notation is as follows:

P_n, n=0,1,2,...,N = pressure jump measured by the pressure sensor after the nth passage of the shock

P_{ij} = pressure jump for the incident shock that would be measured by a sensor located at the surface of end (A).

P_{rj} = same, but for the reflected shock

W_{ij} = same as P_{ij}, but at end (B)

W_{rj} = same as P_{rj}, but at end (B)

P_x, x=a,b,c = absolute pressure; a = ambient pressure, b = pressure after passage of the incident shock, and c = pressure after passage of the reflected shock. Refer to the diagram below, which shows the idealized

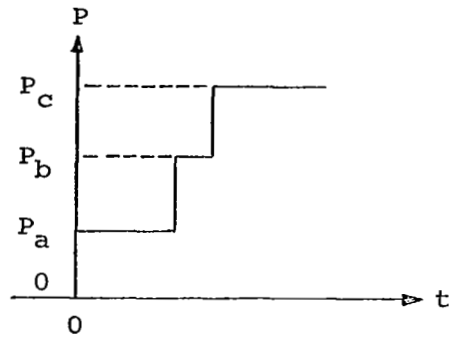

output from an idealized sensor near end (A).

Now the shock strength is defined as

S_{ij} = excess incident shock strength for the jth shock

$$= \frac{P_b - P_a}{P_a} = \frac{P_{ij}}{Pa} = P_{ija} \qquad \text{(Refer To Equation (9))}$$

S_{rj} = excess reflected shock strength for the jth shock

$$= \frac{P_c - P_b}{P_b} = \frac{P_{rj}}{P_b} = \frac{P_{rj}}{P_{ij}+P_a}$$

With this notation the reflection coefficient for pressure* is

$$r = \frac{S_{rj}}{S_{ij}} = \frac{P_{rj}}{P_{ij}+P_a} \frac{P_a}{P_{ij}} = \frac{P_{rj}}{P_{ij}} \frac{1}{1 + P_{ija}}$$

Note that as the incident shock pressure jump P_{ija} becomes small, the expression for r approaches the small signal limit, as required.

---

* A lower case r is used to represent the pressure reflection coefficient, which is related to the energy reflection coefficient by $R = r^2$, from which $\alpha = 1 - r^2$.

Now using these definitions and following the same general procedure to find the pressure jump P_n measured by the pressure sensor after the nth passage of the shock as was followed previously to find the energy ϵ_n remaining in the shock after n passages, we end up with

$$P_n = P_o R_1^{\frac{n}{2}} R_2^{\frac{n}{2}} \prod_{j=1}^{n} (1 + P_{ija}) e^{-n\beta L}$$

Now a rather mild assumption must be made to find an expression for the value of

$$K = \prod_{j=1}^{n} (1 + P_{ija}).$$

The assumption is that the pressure jumps decay exponentially during at least the early portion of the decay process. This is certainly a reasonable assumption, since it is implicit in the very notion of reverberation time absorption measurement. The diagram below depicts a decay curve traced out on a logarithmic level recorder. The symbol T refers to the reverberation time, the time required for the shock pressure jump to decay to 10^{-6} of its inital value.

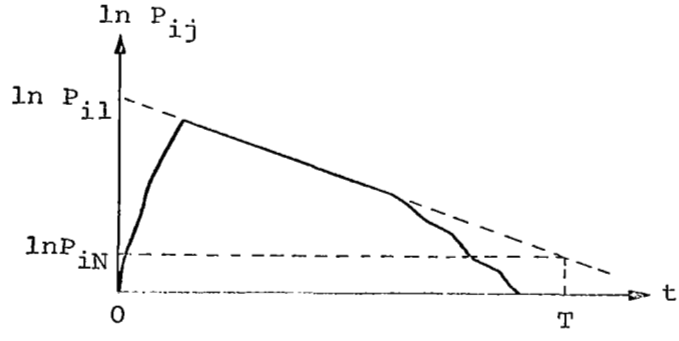

It can easily be shown that

$$P_{ij} = P_{il} e^{-13.8\frac{t}{T}}$$

or, since jL = ct,

$$P_{ija} = P_{ila} e^{\frac{-13.8\ jL}{CT}}$$

Therefore

$$K = \prod_{j=1}^{n} \left(1+P_{ija}\right) = \left(1+P_{ila} e^{\frac{-13.8L}{CT}}\right)\left(1+P_{ila} e^{\frac{-2x13.8L}{CT}}\right)$$

$$x \left(1+P_{ila} e^{\frac{-3x13.8L}{CT}}\right)\cdots\left(1+P_{ila} e^{-13.8}\right)$$

Proceeding as before to find R_s,

$$R_s = \left(\frac{K_o^{\frac{2L}{CT_o}}}{K_s^{\frac{2L}{CT_s}}}\right) e^{\frac{-13.8x2L}{C}\left(\frac{1}{T_s} - \frac{1}{T_o}\right)} \qquad (20)$$

where $$\frac{K_o^{\frac{2L}{CT_o}}}{K_s^{\frac{2L}{CT_s}}} = \frac{\left[\left(1+P_{oa}\ e^{\frac{-13.8L}{CT_o}}\right)\left(1+P_{oa}\ e^{\frac{-2x13.8L}{CT_o}}\right)\right.}{\left[\left(1+P_{oa}\ e^{\frac{-13.8L}{CT_s}}\right)\left(1+P_{oa}\ e^{\frac{-2x13.8L}{CT_s}}\right)\right.}$$

$$x \frac{\left.\left(1+P_{oa}\ e^{\frac{-3x13.8L}{CT_o}}\right)\cdots\left(1+P_{oa}\ e^{-13.8}\right)\right]^{\frac{2L}{CT_o}}}{\cdots\left[\left(1+P_{oa}\ e^{-13.8}\right)\right]^{\frac{2L}{CT_s}}}$$

Equation (20), like equation (19), yields absorption coefficients which are much too low. These results indicate that failure of the shock tube reverberation technique may be fundamental, and due to the fact that a shock wave by its very nature tends to regenerate itself as it propagates. Thus, it may be that the reduction in amplitude resulting from reflection from the absorptive sample is partially offset by this reconstructive process by the time the shock front has traveled a tube length.

Application of the Technique

Figure 29 presents the results of an evaluation of the shock expansion technique with a fiberglass sample. The agreement in this case is excellent, although the results of a similarly performed measurement with a resonant feltmetal absorptive sample are much less positive. Figure 30 shows these results for a driver pressure of 3.1 PSIG compared with the correct results obtained by the tone-burst method at a slightly lower PPL. Tests at higher driver pressures resulted in large data scatter.

Part of the problem was that tube lengths were such that the reflected rarefaction wave was reaching the pressure sensor at nearly the same time as the reflected shock wave.

The shock reflection technique, using the normal, constant area shock tube, was used to measure the variation of r_1, the pressure reflection coefficient of a rigid termination, with time. The results are shown in Figure 31.

The large early scatter may be attributable to interactions with other waves, whereas these processes become averaged out after a greater time lapse and lower pressure so that they are more or less constant over the length of the tube. The high

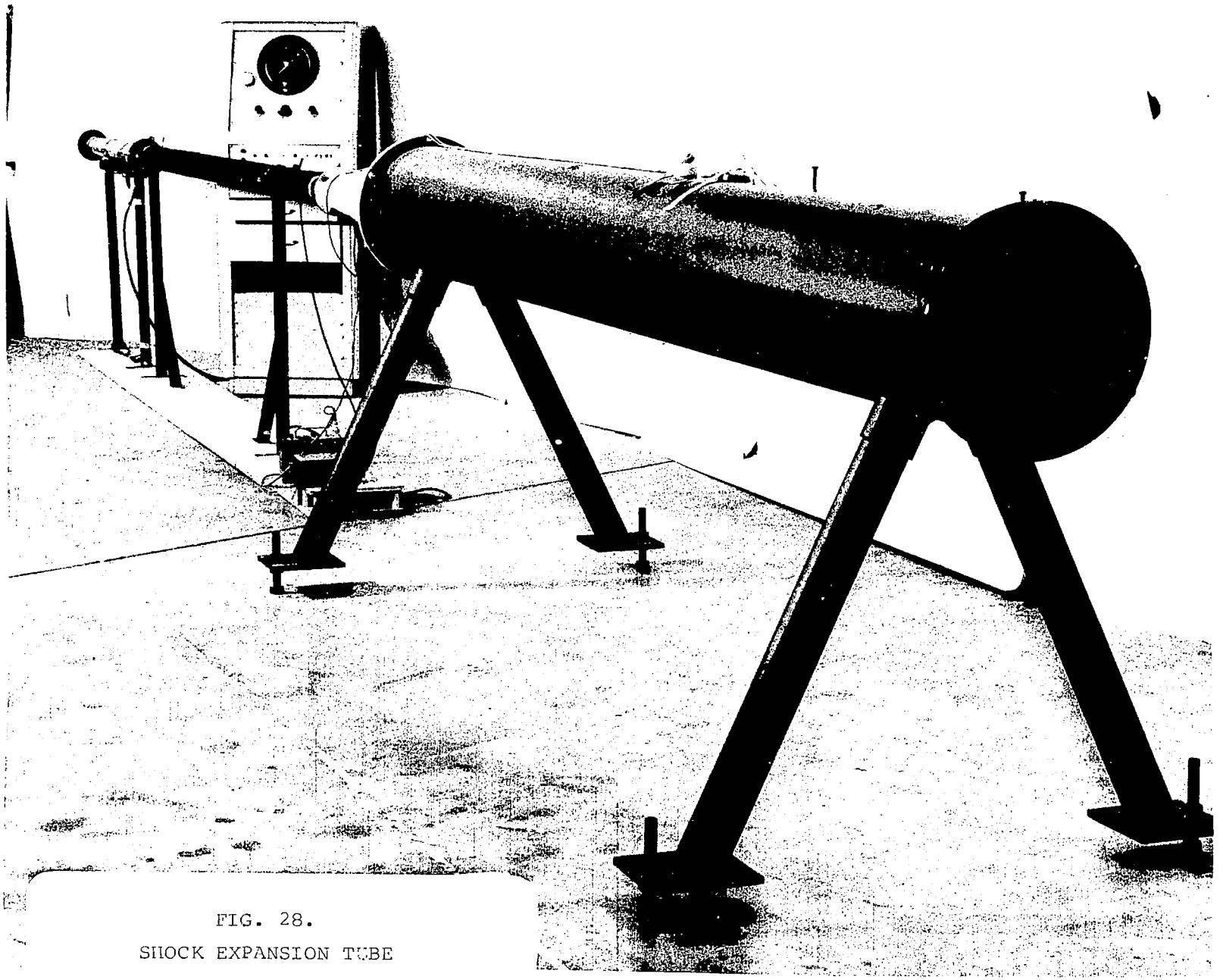

FIG. 28.

SHOCK EXPANSION TUBE

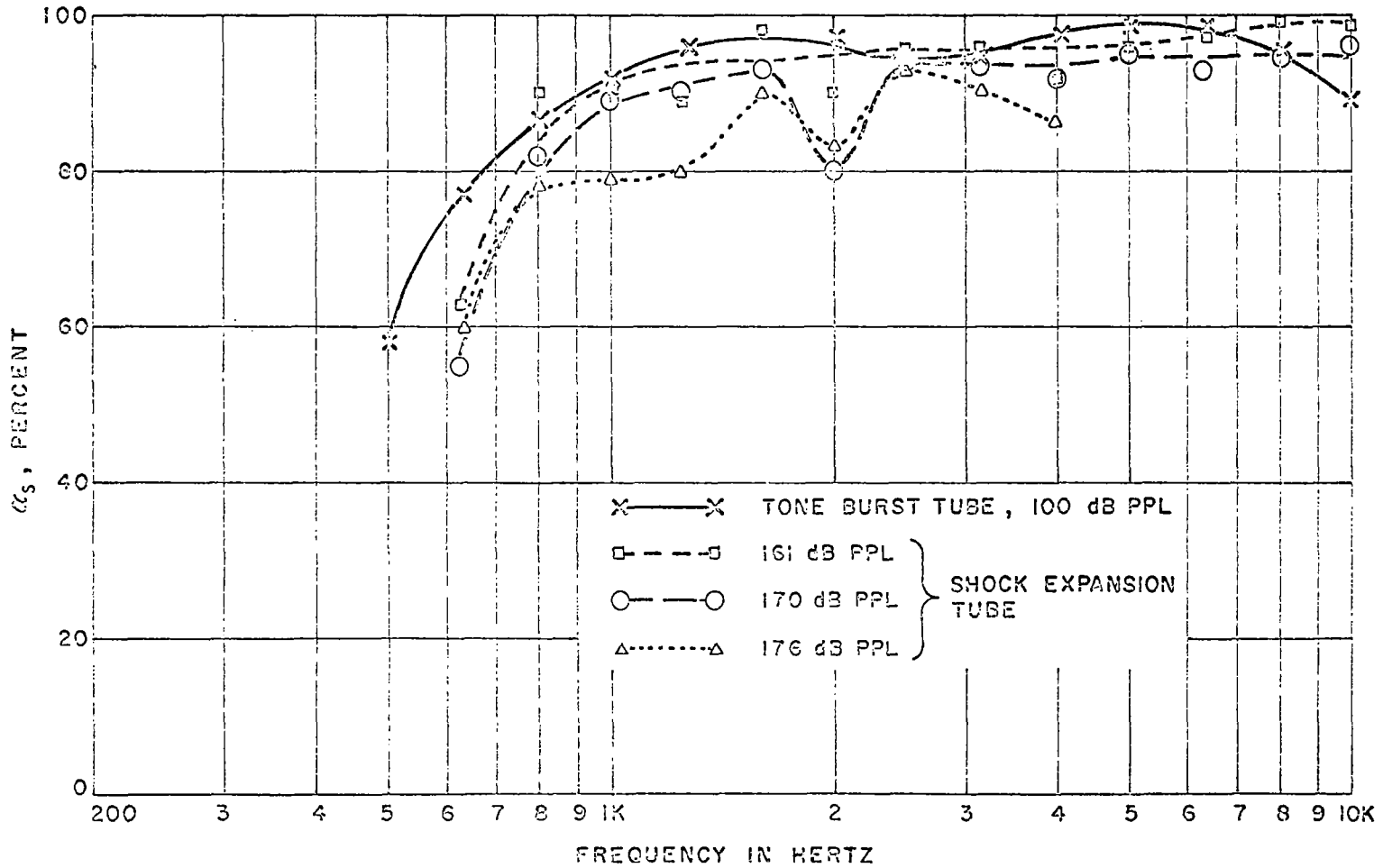

FIG. 29 ABSORPTION COEFFICIENT - FIBERGLASS. COMPARISON OF TONE BURST TUBE AND SHOCK EXPANSION TUBE METHODS

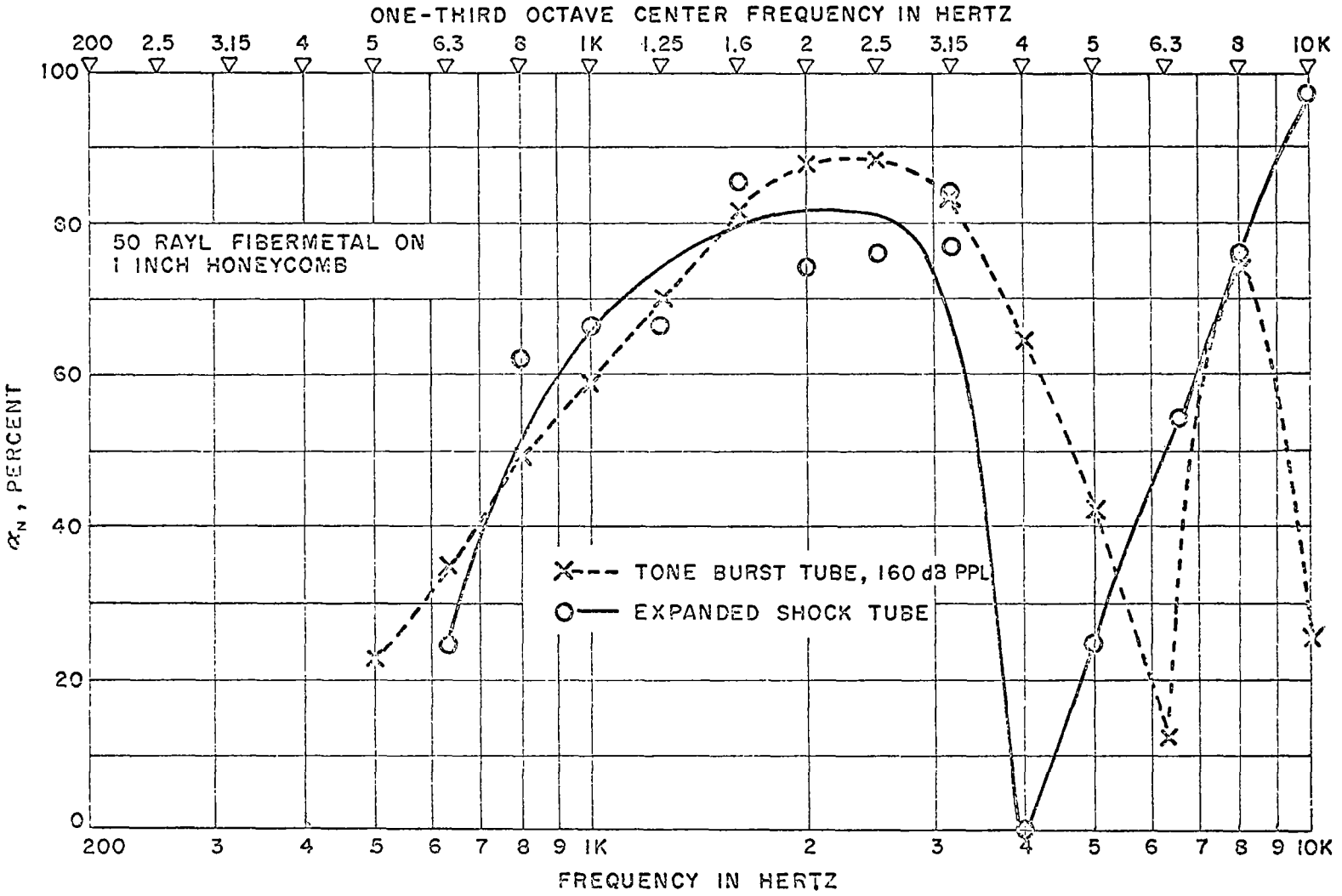

FIG. 30 COMPARISON OF ABSORPTION COEFFICIENT MEASUREMENT BY THE EXPANDED SHOCK AND TONE BURST TUBE METHODS

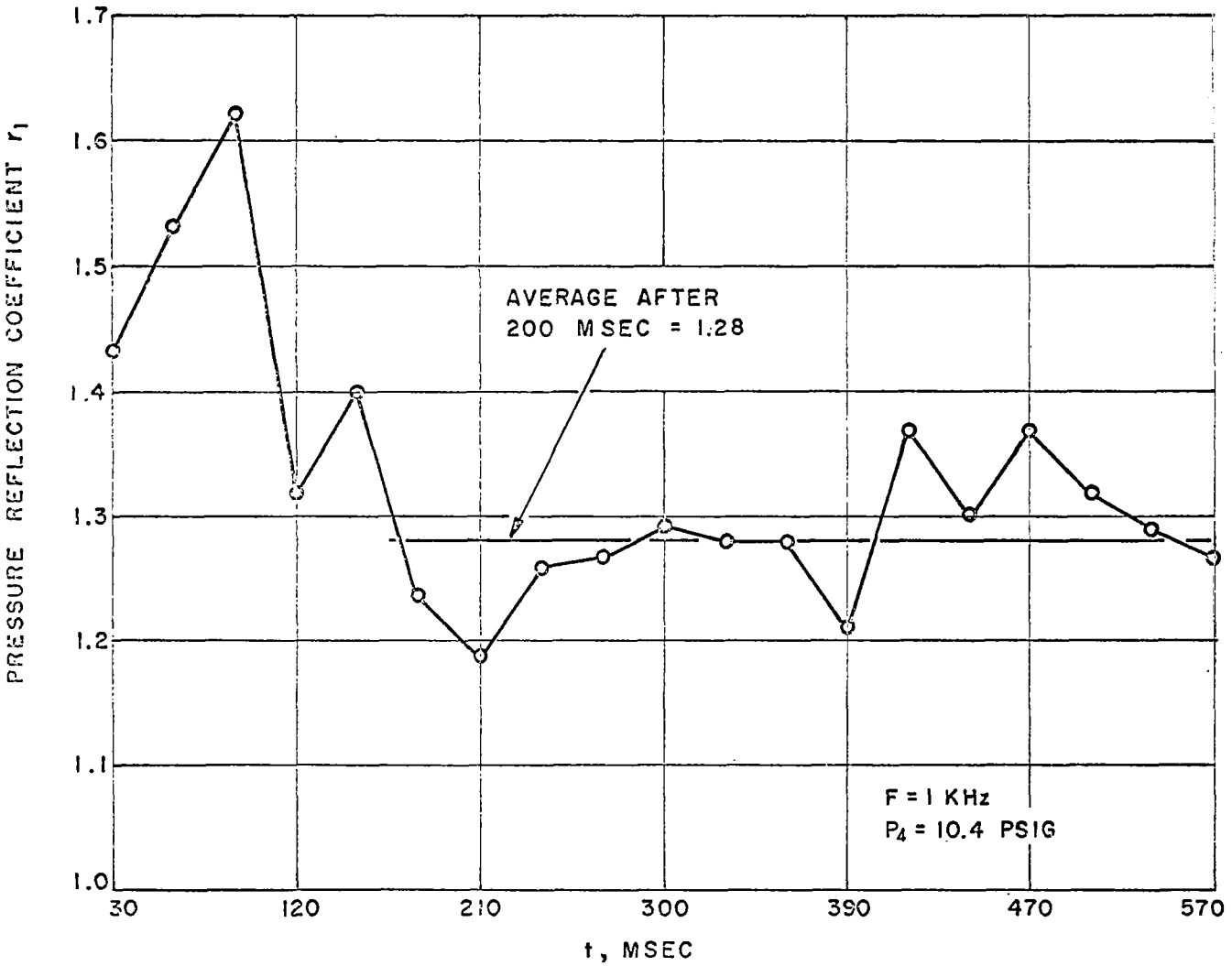

FIG. 31 VARIATION OF THE PRESSURE REFLECTION COEFFICIENT FOR A RIGID TERMINATION WITH TIME

value of the initial reflection cannot be explained by this process, however, and may be due to unaccounted non-linearities. The average value after a 200 msec delay agrees very well with the value obtained by other methods.

Figure 32 shows a similar determination of r_2, the measured pressure reflection coefficient with a fiberglass sample in one end. This quantity is seen to vary much more drastically with time, indicating that non-linearities associated with the early, well-formed shock fronts may be contributing to the failure of the shock tube technique.

Utilizing equation (14) and data of the type shown in Figures 31 and 32, the values of the sample absorption coefficient shown in Figure 33 and 34 are obtained. Figure 31 indicates that the magnitude of the shock strength is not a primary factor influencing the value of α_s. Figure 34 shows that plots of α_s versus time tend to converge to a value which is in reasonable agreement with the value obtained with an impedance tube.

Thus, while this technique is apparently capable of yielding correct values of absorption coefficient, the procedure is so experimentally awkward as to render it impractical as an analytical laboratory tool.

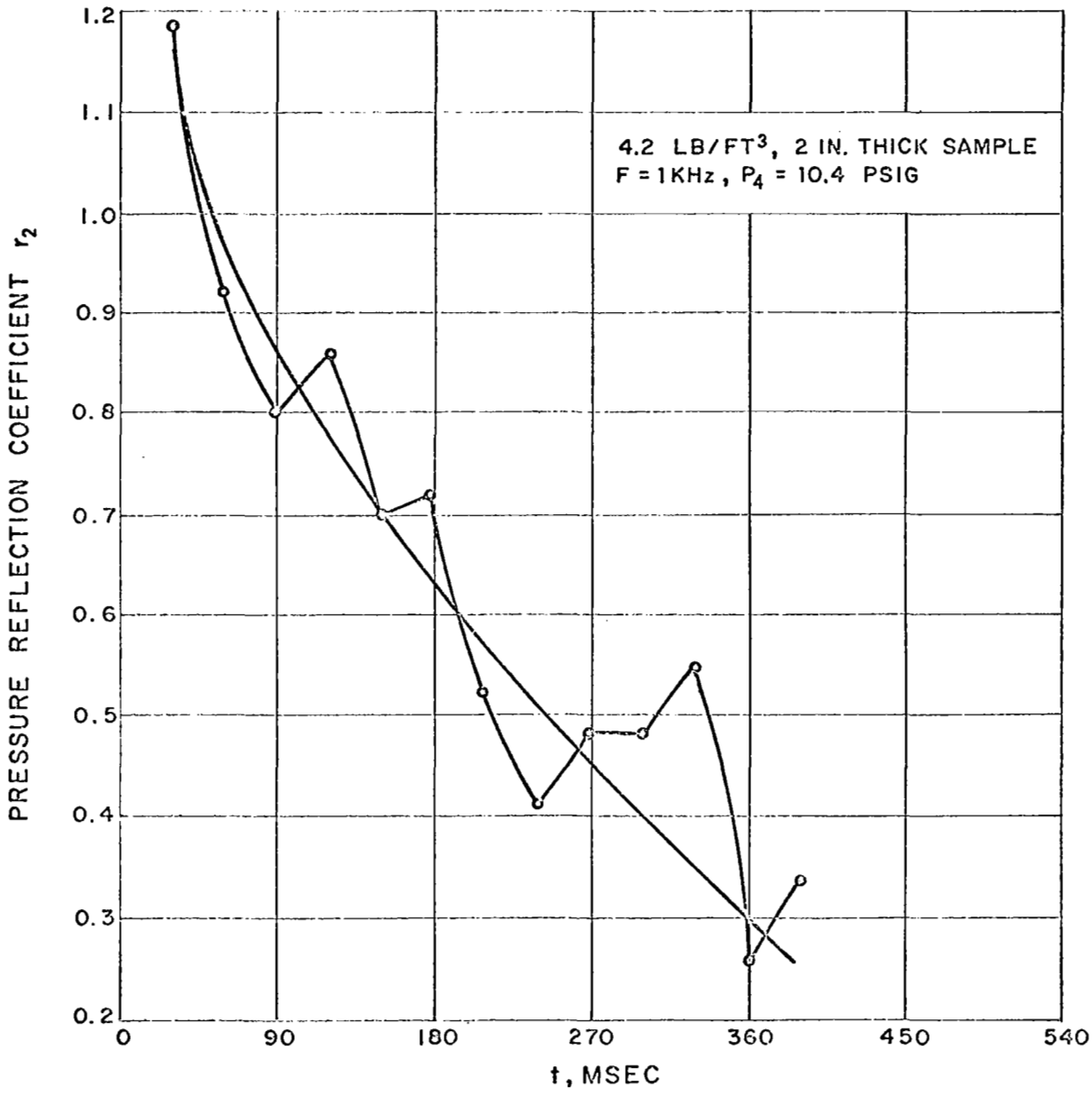

FIG. 32 VARIATION OF THE MEASURED PRESSURE REFLECTION COEFFICIENT FOR A FIBERGLASS SAMPLE WITH TIME

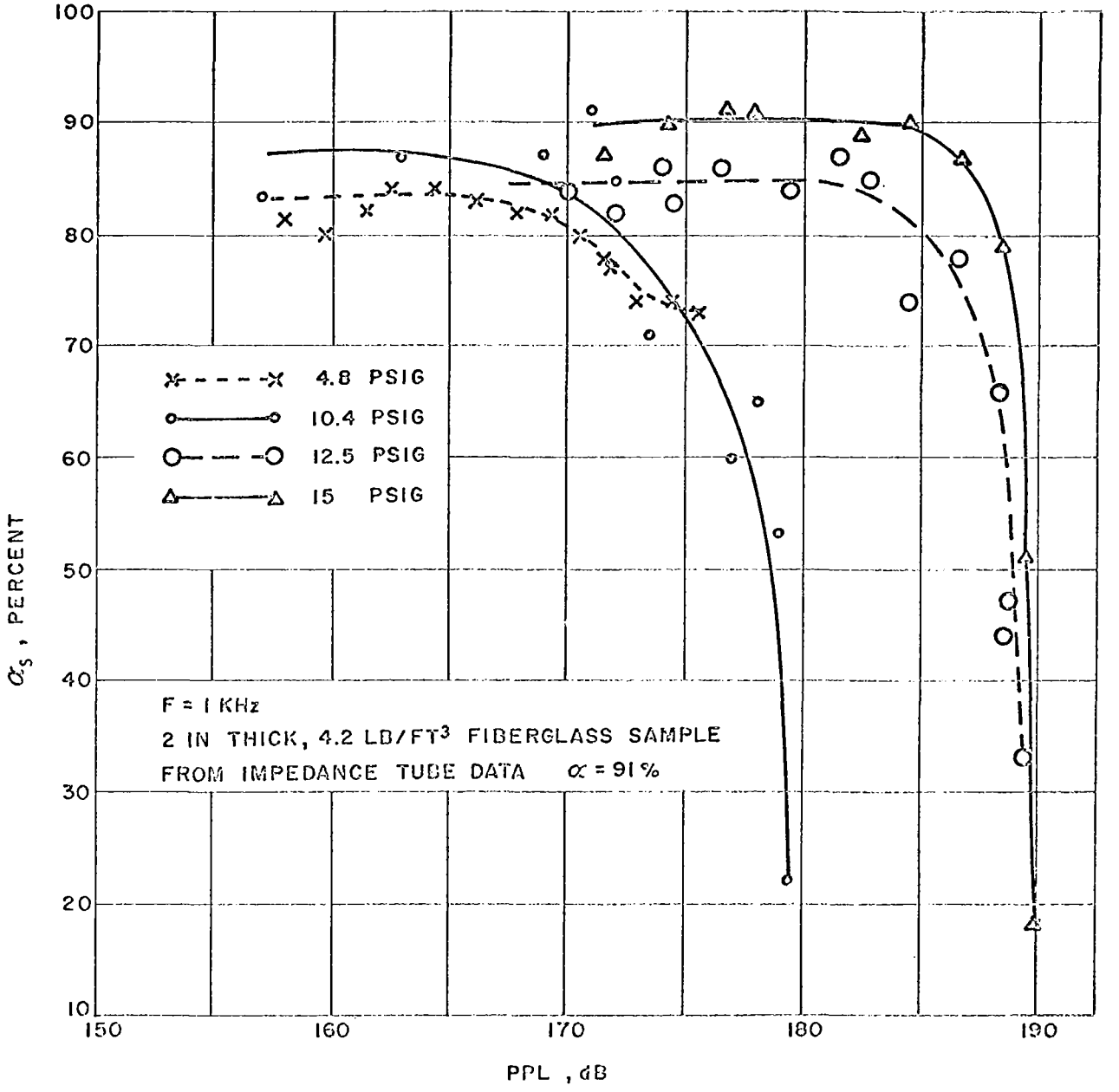

FIG. 33. VARIATION OF SAMPLE ABSORPTION COEFFICIENT WITH INCIDENT SHOCK OVERALL PPL AND P_4

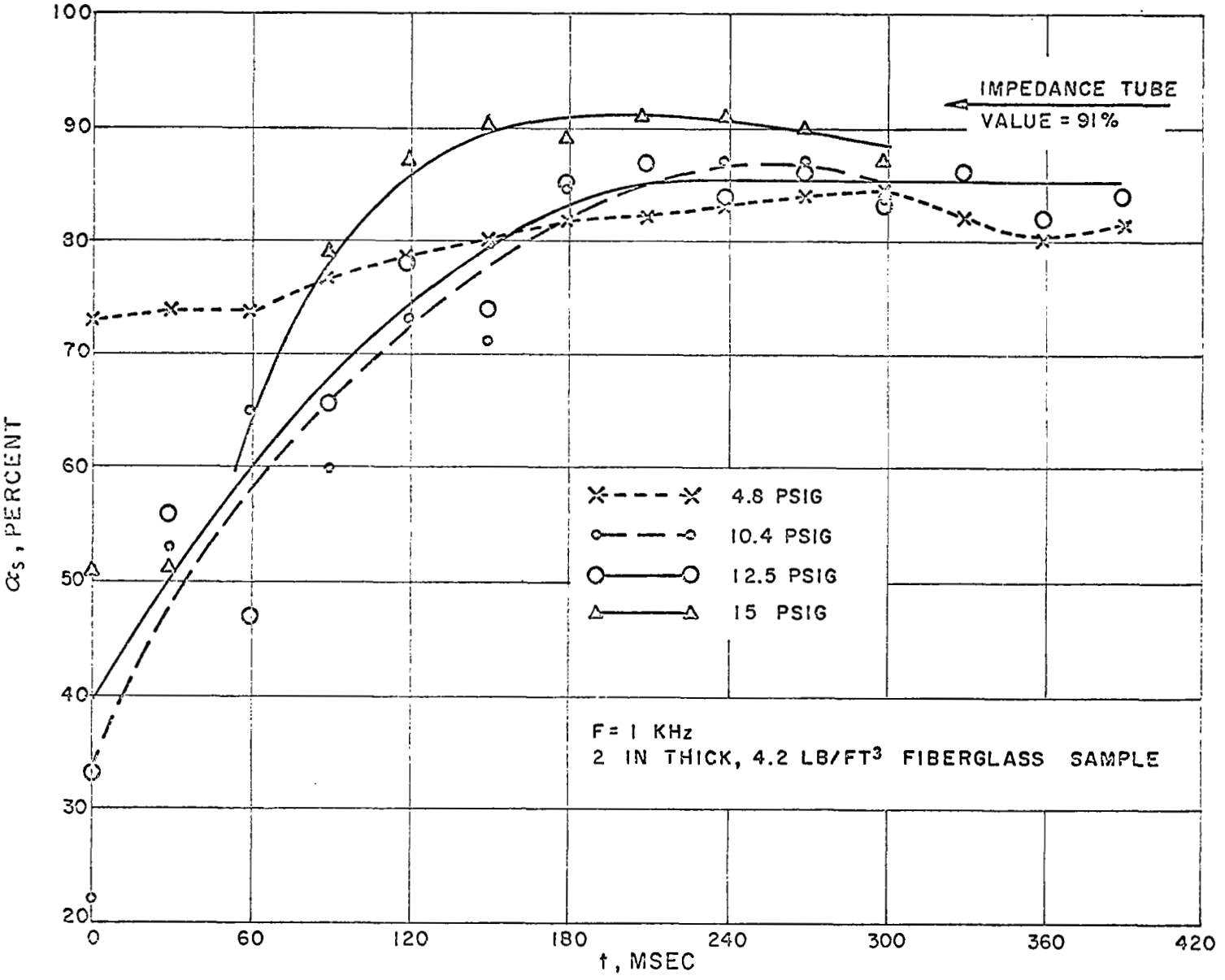

FIG. 34. VARIATION OF SAMPLE ABSORPTION COEFFICIENT WITH TIME AND P_4

CONCLUSIONS

Tone Burst Tube Procedure

The tone burst tube technique of absorption measurement has been developed into a unique and useful laboratory tool. The utility of the technique has been demonstrated by measuring the absorption coefficient of feltmetal, sintered bronze, fiberglass, and Scottfoam, and comparing the results with data obtained on the same materials with an impedance tube. In addition, the measurements on these materials have been extended to higher intensities than the impedance tube is capable of achieving to demonstrate the non-linearity of the absorption with sound intensity. The measured non-linearity has conformed with expectations in every respect. It is therefore felt that this technique has been demonstrated to be a valid and reliable method of absorption measurement.

It has been established that sample size is unimportant, subject to the constraint that sample diameter remain less than half a wavelength at the highest frequency of interest. This restriction also places an upper limit on the frequency range; the lower limit is dictated by the requirement that the incident and reflected pulse do not overlap in time at the microphone location. In other words, tube length places the lower bound on the frequency range.

During this program PPL was limited by transducer and amplifier capabilities. In all cases, commercially available equipment was employed. Modified or specially designed drivers and a special power amplifier output stage could have significantly increased the maximum PPL.

While the technique is not directly applicable to the case of grazing incidence or superimposed air flow, these situations can be accommodated by utilizing the tone burst signal in a transmission attenuation, rather than a reflection coefficient, measurement mode.

Shock Tube Technique

The shock expansion technique, wherein a shock wave is weakened by expansion through an area transformation, appears capable of successfully measuring the absorption coefficient of materials. The results of limited experimentation were extremely encouraging.

The shock tube reverberation technique appears to be unsuitable for absorption measurement. It is felt that this is because a shock front tends to reconstruct itself as it propagates, thereby partially negating spectral absorption by the sample.

The basic concept of using shock waves for this measurement immediately implies that extremely high PPL's can easily be generated. In light of this fact, it is recommended that further experimentation be performed on the shock expansion technique.

REFERENCES

1. Herschel A. Watson, Jr., "Structural and Environmental Studies of Duct-Lining Acoustical Materials," Douglas Paper 5544, Noise Abatement Symposium of the 1969 Southern Metal Conference, Grand Bahama Island, April 1969.

2. W. E. Zorumski and T. L. Parrott, "Nonlinear Acoustic Theory for Thin Porous Sheets," NASA SP-189, 1968, pp 17-27.

3. R. A. Mangiarotty, "Acoustic Lining Concepts and Materials for Engine Ducts," J. Acoust. Soc. Amer. 77, 1 (Part 1), p.77(A) (1969).

4. J. Atvars and R. A. Mangiarotty, "Duct Acoustic Lining Technology for Applications to Turbofan Engines," ibid., p.78(A)

5. Alan H. Marsh, I. Elias, J. C. Hoehne, and R. L. Grasca, "A Study of Turbofan-Engine-Compressor-Noise-Suppression Techniques," NASA CR-1056, June 1968.

6. Athanasios Papoulis, The Fourier Transform and its Applications, McGraw-Hill Book Co., New York, 1962.

7. R. A. Mangiarotty, A. H. Marsh, and E. Feder, "Duct Lining Materials and Concepts," NASA SP-189, pp. 29-52, 1968.

8. H. E. Dahlke, G. T. Kantarges, T. E. Siddon, and J. J. Van Houten, "The Shock Expansion Tube and Its Application as a Sonic Boom Simulator," NASA Report No. CR-1055, June 1968.

9. I. I. Glass, et al, "A Theoretical and Experimental Study of the Shock Tube," UTIA Report No. 2 (November 1953); also Glass and Hall, Handbook of Supersonic Aerodynamics, Section 18, Shock Tubes, NAVORD Report 1488 (Vol. 6) December 1959.

10. M. R. Schroeder, "Some New Results in Reverberation Theory and Measurement Methods," Paper G31, 5th International Congress of Acoustic, Liege, September 1965.

11. G. Millington, "A Modified Formula for Reverberation," J. Acoust. Soc. Amer. 4, 1, pp. 69-82 (July 1932).

12. Robert W. Young, "Sabine Reverberation Equation and Sound Power Calculations," J. Acoust. Soc. Amer. 31, 7, pp. 912-921 (July 1959).

13. Carl F. Eyring, "Methods of Calculating the Average Coefficient of Sound Absorption," J. Acoust. Soc. Amer. 4, 3, pp. 178-192 (January 1933).

NASA-Langley, 1971 — 22 CR-1698